NASA Technical Memorandum 81941

(NASA-TM-81941) A CRACK-CLOSURE MODEL FOR PREDICTING FATIGUE-CRACK GROWTH UNDER AIRCRAFT SPECTRUM LOADING (NASA) 63 p
HC A04/MF A01 CSCL 20K
N81-18412
Unclas
G3/39 41485

A CRACK-CLOSURE MODEL FOR PREDICTING FATIGUE-CRACK GROWTH UNDER AIRCRAFT SPECTRUM LOADING

J. C. Newman, Jr.

January 1981

National Aeronautics and
Space Administration

Langley Research Center
Hampton, Virginia 23665

SUMMARY

Experiments on metallic materials have shown that fatigue cracks remain closed during part of the load cycle under constant- and variable-amplitude loading. These experiments have shown that crack closure is a significant factor in causing load-interaction effects (retardation and acceleration) on crack-growth rates under variable-amplitude loading.

The present paper is concerned with the development and application of an analytical model of cyclic crack growth that includes the effects of crack closure. The model was based on a concept like the Dugdale model, but was modified to leave plastically-deformed material in the wake of the advancing crack tip.

The model was used to correlate crack-growth rates under constant-amplitude loading, and to predict crack growth under aircraft spectrum loading on 2219-T851 aluminum alloy sheet material. The predicted crack-growth lives agreed well with experimental data. The ratio of predicted-to-experimental lives ranged from 0.66 to 1.48. These predictions were made using data from an ASTM E24.06.01 Round Robin.

INTRODUCTION

Experiments [1] on metallic materials have shown that fatigue cracks remain closed during part of the load cycle under constant- and variable-amplitude loading. The crack-closure concept has been used to correlate crack-growth rates under constant-amplitude loading [2] and is a significant factor in causing load-interaction effects on crack-growth rates (retardation and acceleration) under variable-amplitude loading. Crack-closure is caused by residual plastic deformations remaining in the wake of an advancing crack. Measurements of crack-opening stresses are very difficult and have been made on only a few materials and for a limited number of loading variables. To develop the rationale for predicting crack growth under general cyclic loading, a mathematical model of crack closure must be developed and verified for constant- and variable-amplitude loading.

The crack-closure phenomenon has been analyzed using two-dimensional, elastic-plastic, finite-element methods [3-6]. The finite-element analyses were shown to be quite accurate, but were very complicated and required large computing facilities. There have also been several attempts to develop simple analytical models of crack closure [3,7-11]. All of these models were based on a concept like the Dugdale model [12] or strip-yield model, but modified to leave plastically-deformed material in the wake of the advancing crack. Newman [3], Budiansky and Hutchinson [8], and Führing and Seeger [10,11] studied only the crack-closure behavior. But, Dill and Saff [7] and Hardrath, Newman, Elber and Poe [9] used the crack-opening stresses from the models to predict crack growth under spectrum loading. However, none of these studies considered the influence of three-dimensional constraint on the crack-closure behavior.

The purpose of the present paper is to develop and apply an analytical crack-closure model that simulates plane-stress and plane-strain conditions. The present model was based on the Dugdale model, but was modified to leave plastically-deformed material along the crack surfaces as the crack advances. Plane-stress and plane-strain conditions were simulated by using a "constraint" factor on tensile yielding to account for three-dimensional effects.

The model was developed for a central crack in a finite-width specimen that was subjected to uniformly applied stress. The model was exercised under constant-amplitude loading using various applied stress levels and stress ratios. The crack-opening stresses calculated from the model were used to calculate Elber's effective stress-intensity factor range [1]. Experimental crack-growth rates from 2219-T851 aluminum alloy sheet material under constant-amplitude loading were correlated with the effective stress-intensity factor range for a wide range of stress levels and stress ratios. The experimental data were obtained from Chang and Stolpestad [13]. An equation relating crack-growth rate to effective stress-intensity factor range, threshold stress-intensity factor range, and fracture toughness has been developed for the complete range of crack-growth rates. The closure model was then used to predict crack growth in 2219-T851 aluminum alloy material under aircraft spectrum loading [13]. The predictions were made using the closure model under nearly plane-strain conditions. These predictions were made using data from an ASTM E24.06.01 Round Robin. The purpose of the round robin was to compare various methods for predicting crack growth in 2219-T851 aluminum alloy center-crack tension specimens subjected to aircraft spectrum loading.

LIST OF SYMBOLS

b_k	dimensions for partially-loaded crack ($k = 1,2$), m
C_k	material crack-growth constants ($k = 1,5$)
c	half-length of crack, m
c_f	half-length of final crack, m
c_i	half-length of initial crack, m
c_n	half-length of starter notch, m

d	half-length of crack plus tensile plastic zone, m
E	Young's modulus of elasticity, MPa
F	boundary-correction factor on stress intensity
K	stress-intensity factor, MPa-m$^{1/2}$
K_{Ie}	stress-intensity factor at failure, MPa-m$^{1/2}$
K_{max}	maximum stress-intensity factor, MPa-m$^{1/2}$
K_F	elastic-plastic fracture toughness, MPa-m$^{1/2}$
L_i	length of element (i) created by plastic deformation, m
m	fracture toughness parameter
N	number of cycles
N_P	number of cycles predicted from analysis
N_T	number of cycles from test specimen
n	total number of bar elements
R	stress ratio (S_{min}/S_{max})
S	applies stress, MPa
S_{max}	maximum applied stress, MPa
S_{min}	minimum applied stress, MPa
S_o	crack-opening stress, MPa
t	specimen thickness, m
V	crack-surface displacement, m
W	specimen width, m
w_i	half-width of bar element at point i, m
x,y	Cartesian coordinates
x_i	coordinate location for element i, m
α	constraint factor, $\alpha = 1$ for plane stress and $\alpha = 3$ for plane strain

Δc^*	crack-growth increment over which S_o is held constant
ΔK	stress-intensity factor range, MPa-m$^{1/2}$
ΔK_{eff}	effective stress-intensity factor range, MPa-m$^{1/2}$
ΔK_o	effective threshold stress-intensity factor range, MPa-m$^{1/2}$
ΔK_{th}	threshold stress-intensity factor range, MPa-m$^{1/2}$
ΔS_{eff}	effective stress range, MPa
η	material constant, $\eta = 0$ for plane stress and $\eta = \nu$ for plane strain
ν	Poisson's ratio
ρ	length of tensile plastic zone, m
σ_j	stress on segment of crack surface, MPa
σ_o	flow stress (average between σ_{ys} and σ_u), MPa
σ_{ys}	yield stress (0.2 percent offset), MPa
σ_u	ultimate tensile strength, MPa
ω	length of compressive plastic zone, m

ANALYTICAL CRACK-CLOSURE MODEL

To calculate crack-closure and crack-opening stresses during crack propagation, the elastic-plastic solution for stresses and displacements in a cracked body must be known. The crack-surface displacements, which are used to calculate contact (or closure) stresses during unloading, are influenced by plastic yielding at the crack tip and residual deformations left in the wake of the advancing crack. Upon reloading, the applied stress level at which the crack surfaces become fully open (no surface contact) is directly related to contact stresses. This stress is called the "crack-opening stress."

Because there are no closed-form solutions for elastic-plastic cracked bodies, simple approximations must be used. As previously mentioned, the present model was based on the Dugdale model. In the proposed model, several assumptions about the plastic zone, the material cyclic stress-strain behavior, the residual plastic deformations, and crack extension were made. Some of these assumptions are discussed in the following sections and the others, along with details, are discussed in appendix A.

The model developed herein was for a central crack in a finite-width plate subjected to uniform applied stress, as shown in figure 1. The model was based on the Dugdale model, but was modified to leave plastically-deformed material in the wake of the advancing crack. The primary advantage in using this model is that the plastic-zone size and crack-surface displacements are obtained by superposition of two elastic problems. These two elastic problems, a crack in a finite-width plate subjected to either remote uniform stress, S, or to a uniform stress, σ, applied over a segment of the crack surface, are shown in figure 2. The stress-intensity factor and crack-surface displacement equations for these loading conditions are given in appendix B.

Figure 3 shows a schematic of the model at maximum and minimum applied stress. The model was composed of three regions: (1) a linear elastic region containing a fictitious crack of half-length $c + \rho$, (2) a plastic region of length ρ, and (3) a residual plastic deformation region abong the crack surfaces. The physical crack is of half-length c. Region 1 was treated as an elastic continuum, and the crack-surface displacements under various loading conditions are given in appendix B. Regions 2 and 3 were composed of rigid-perfectly plastic (constant stress) bar elements with a flow stress, σ_o, which is the average between the yield stress, σ_{ys}, and the ultimate tensile strength, σ_u. The shaded regions in figure 3(a) and 3(b) indicate material which is in a plastic state. At any applied stress level, the bar elements are either intact (in the plastic zone) or broken (residual plastic deformation). The broken elements carry compressive loads only, and then only if they are in contact. The elements in contact yield in compression when the contact stress reaches $-\sigma_o$. Those elements that are not in contact do not affect the calculation of crack-surface displacements. To account for the effects of state-of-stress on plastic-zone size, a constraint factor α was used to elevate the tensile flow stress for the intact elements in the plastic zone. The effective flow stress $\alpha\sigma_o$ under simulated plane-stress conditions was σ_o and under simulated plane-strain conditions was $3\sigma_o$. The constraint factor is a lower bound for plane stress and an approximate upper bound for plane strain. (Although the Dugdale model is not entirely suited for plane strain yielding, the size of the plastic zone at the crack tip and its influence on crack-surface displacements may be adequate.) These constraint factors were verified using elastic-plastic finite-element analyses of cracked bodies under plane-stress [6] and plane-strain conditions (by the author). The procedure used to establish the constraint factor (α) is discussed later.

The analytical crack-closure model, discussed in appendix A, was used to calculate crack-opening stresses, S_o, as a function of crack length and load history. In turn, the crack-opening stress was used to calculate the effective stress-intensity factor range, as proposed by Elber, and, consequently, the crack-growth rates.

FATIGUE-CRACK GROWTH RATE EQUATION

The crack-growth equation proposed by Elber [2] states that the crack-growth rate is a power function of the effective stress-intensity factor range only. Later, Hardrath, Newman, Elber and Poe [9] showed that the power law was inadequate at high growth rates approaching fracture. The results presented herein show that it is also inadequate at low growth rates approaching threshold. To account for these effects, the power law was modified to

$$\frac{dc}{dN} = C_1 \, \Delta K_{eff}^{C_2} \, \frac{1 - \left(\frac{\Delta K_o}{\Delta K_{eff}}\right)^2}{1 - \left(\frac{K_{max}}{C_5}\right)^2} \tag{1}$$

where

$$\Delta K_o = C_2 \left(1 + C_4 \frac{S_o}{S_{max}}\right) \tag{2}$$

$$K_{max} = S_{max} \sqrt{\pi c} \; F \tag{3}$$

and

$$\Delta K_{eff} = (S_{max} - S_o) \sqrt{\pi c} \; F \tag{4}$$

The crack-opening stresses, S_o, were calcualted from the analytical closure model. Equation (1) gives the "sigmoidal" shape commonly observed when fatigue crack-growth rate data are plotted against stress-intensity factor range. In the intermediate range of crack-growth rates, equation (1) is basically Elber's proposed power law, $C_1 \, \Delta K_{eff}^{C_2}$. The constants C_1 to C_5 were determined to best fit experimental data for constant-amplitude loading.

The coefficients C_3 and C_4 were determined from threshold data on the 2219-T851 aluminum alloy sheet material from reference [14]. The effective threshold stress-intensity factor range, ΔK_o, was determined from the threshold stress-intensity factor range, ΔK_{th}, as

$$\Delta K_o = U \, \Delta K_{th} = \frac{1 - \dfrac{S_o}{S_{max}}}{1 - R} \, \Delta K_{th} \qquad (5)$$

The coefficient C_5 is the elastic stress-intensity factor at failure or cyclic fracture toughness. The coefficient C_5 was chosen to be 77 MPa-m$^{1/2}$ (70 ksi-in$^{1/2}$) on the basis of the crack-growth tests in reference [13] (see appendix C).

The coefficients C_1 and C_2 were found from constant-amplitude rate data [13], after C_3, C_4 and C_5 were determined, by using a least-squares regression analysis. The constant-amplitude correlations were made using S_o values computed from the model with various constraint factors.

It was found that an α of about 2.3 would give a good correlation. A summary of the coefficients used to correlate the constant-amplitude data under nearly plane-strain conditions ($\alpha = 2.3$ and $\eta = 0$) are as follows:

$$\left.\begin{aligned} C_1 &= 1.764 \times 10^{-10} \quad (9.378 \times 10^{-9}) \\ C_2 &= 3.18 \\ C_3 &= 2.97 \text{ MPa-m}^{1/2} \quad (2.7 \text{ ksi-in}^{1/2}) \\ C_4 &= 0.8 \\ C_5 &= 77 \text{ MPa-m}^{1/2} \quad (70 \text{ ksi-in}^{1/2}) \end{aligned}\right\} \qquad (6)$$

When SI units are used, ΔK_{eff} and K_{max} are given in MPa-m$^{1/2}$ and dc/dN is given in m/cycle. When U.S. Customary are used, ΔK_{eff} and K_{max} are given in ksi-in$^{1/2}$ and dc/dN is given in in/cycle.

Figure 4 shows a comparison between experimental growth rates [13] and growth rates calculated with equation (1) for the 2219-T851 aluminum alloy material. These constant-amplitude data were for R ratios between -1 and 0.7, and maximum-stress-to-yield-stress ratios of 0.15 to 0.77. Data generated when the net-section stress exceed the yield stress were not included. For the 2219-T851 aluminum alloy material, the yield stress (σ_{ys}) was 360 MPa (52 ksi) and the ultimate tensile strength (σ_u) was 455 MPa (66 ksi). The dashed lines show factor-of-2 bands about the perfect agreement line. Most of the data were well within these bands.

Figure 5 shows a plot of ΔK against dc/dN for several R ratios for 2219-T851 aluminum alloy material to illustrate the sigmoidal shape of equation (1). The experimental data were obtained from reference [14]. The curves were calculated from equation (1). The $R = -1$ data were obtained from a small center-crack tension specimen ($W = 76.2$ mm) and the other data were obtained from small compact specimens ($W = 50.8$ mm). The crack-growth coefficients (C_1, C_2, C_3 and C_4) used to calculate the curves were identical to those shown in equations (6). However, the coefficient C_5 for the small compact specimens was 38.5 MPa-m$^{1/2}$ and for the small center-crack specimen was 55 MPa-m$^{1/2}$. The coefficients (C_5) were calculated from the Two-Parameter Fracture Criterion [15] using $K_F = 550$ MPa-m$^{1/2}$ and $m = 1$. These values of K_F and m were obtained from the final crack lengths and maximum stress levels used in the constant-amplitude tests from reference [13], (see appendix C). The calculated curves and the experimental data are in good agreement.

APPLICATION OF THE CRACK-CLOSURE MODEL AND RATE EQUATION

The analytical crack-closure model and crack-growth program (FAST - Fatigue Crack Growth Analysis of Structures) was applied to constant-amplitude and aircraft-spectrum loading on 2219-T851 aluminum alloy sheet material.

Under constant-amplitude loading, the model was exercised under simulated plane-stress and plane-strain conditions. Some typical examples of crack-surface displacements at maximum load and of crack-surface contact stresses at minimum load are given. Calculated crack-opening stresses are shown as a function of crack length, stress ratio, stress level, and constraint factor (α). The calculated crack-growth lives under various constant-amplitude loading are compared with experimental data.

Because most crack-growth life is generated at small crack lengths and low stess levels (plastic-zone size is small compared to sheet thickness), nearly plane-strain conditions ($\alpha = 2.3$) were found to give a good correlation under constant-amplitude loading. These conditions were also used to predict crack-growth life under aircraft spectrum loading. The crack-opening stresses were calculated from the model as a function of crack length and load history, and the crack-growth rates were predicted from equation (1). The predicted lives under various spectrum loadings are compared with experimental data in the following sections.

Constant-Amplitude Loading

Crack-surface displacements and contact stresses.- The normalized crack-surface displacements, EV/Sd, at maximum applied stress under constant-amplitude loading are shown as a function of coordinate location, x/d, in figure 6(a). The shaded region shows the plastic and residual deformations at maximum stress after simulated crack extension. The residual deformations along the crack surfaces are of nearly uniform length. The newly created crack-tip element comes into contact after very slight unloading. The normalized contact stresses (σ_j/σ_o) at minimum applied stress ($S_{min} = 0$) are shown in figure 6(b). The elements are in contact all along the crack surfaces, but only the elements near the crack tip carry significant loads. The elements near the crack tip yield in compression, whereas those near $x = d$ are in tension. For x greater than d, the stresses (not shown) are in tension but rapidly drop to the applied stress, S_{min}, as x increases.

Crack-opening stresses.- The crack-opening stresses are calculated from the contact stresses at minimum load as shown in appendix A. In figure 7, some typical crack-opening stresses are shown as functions of crack length. Results are shown for three stress levels used in the constant-amplitude tests ($R = 0$). At low stress levels the crack-opening stresses rapidly reach a "stabilized" level. However, at the highest stress level (276 MPa) the crack-opening stresses did not stabilize but did oscillate about a mean level for most of the simulated test. The sharp changes in S_o at certain crack lengths were due to the element "lumping" procedure described in appendix A. Basically, this procedure lumps adjacent elements together to form a single element to keep the total number of elements to reasonable size and to save computer time. (The sharp changes in S_o can be eliminated by using smaller elements.) These sharp changes in S_o have less than 1 percent effect on the effective stress range. In the constant-amplitude crack-growth rate correlation (fig. 4), the stabilized crack-opening stresses or the average values (shown by the dashed lines) were used.

The variation of stabilized (or average) crack-opening stresses with stress ratio, R, for $S_{max} = \sigma_o/3$ is shown in figure 8. The curves show how S_o/S_{max} varies as conditions change from simulated plane stress ($\alpha = 1$) to simulated plane strain ($\alpha = 3$). At any R ratio, the S_o/S_{max} values are lower for higher values of α. At $R = 0$, the crack-opening stress was about 0 47 S_{max} for plane stress and was about 0.25 S_{max} for plane strain. These results are in good agreement with finite-element analyses under plane-stress [6] and plane-strain conditions (by the author). At negative R ratios, S_o/S_{max} appears to be a linear function of the R ratio. At positive R ratios, S_o/S_{max} rapidly approaches the dashed line. For R ratios greater than about 0.7, S_o/S_{max} equals S_{min}/S_{max}, and the values are also independent of the constraint factor.

The influence of the maximum applied stress level on crack-opening stresses are shown in figure 9. At the lower R ratios, the maximum applied stress had a dramatic affect on crack-opening stresses, but at an R ratio of 0.7 the maximum applied stress had no influence. The influence of the maximum applied stress was more pronounced under plane-stress conditions (dashed curves) than under plane-strain conditions (solid curves).

Crack-growth calculations.- Table 1 shows the experimental lives (N_T) and the ratio of calculated to experimental crack-growth lives (N_p/N_T) from the initial crack length c_i to the final crack length c_f, for the constant-amplitude tests on 2219-T851 aluminum alloy material. The closure model used $\alpha = 2.3$. The ratio N_p/N_T ranged from 0.64 to 2.09. The lowest and highest values of N_p/N_T were obtained from the tests conducted at the highest stress level. The mean value of N_p/N_T was 1.06 and the standard deviation was 0.34 for all tests shown in table 1, except the low stress level (55 MPa) test with $R = -0.3$.

The two tests indicated, by footnote (b) in table 1, were not used in obtaining the crack-growth constants (C_1 and C_2). The 55 MPa and $R = -0.3$ crack-length-against-cycles curve did not agree with two other tests in reference [13] at the same stress level and stress ratio. The 276 MPa and negative R ratio (-0.3) test was not included because, during the simulated test, the calculated S_o values did not stabilize with increasing crack length.

Spectrum Loading

Crack-surface displacements and contact stresses.- The normalized crack-surface displacements at maximum applied stress, and the normalized contact stresses at minimum applied stress under a typical spectrum loading, are shown as a function of coordinate location in figure 10. The displacement profile is quite similar to that shown for constant-amplitude loading (fig. 6(a)), but small differences in the displacement profile cause large differences in contact stresses, as shown in figure 10(b). The calculated crack-opening stresses reflect the influence of these irregular contact stresses on subsequent crack growth.

Crack-opening stresses.- The variation of crack-opening stress with crack length for a typical spectrum loading test is shown in figure 11. The half-length of the elox notch (c_n) was 3.2 mm. The specimen was cycled under constant-amplitude loading ($S_{max} = 69$ MPa) at $R = 0$ until the crack grew to a crack half-length (c_i) of 3.8 mm. Next, a typical fighter spectrum was applied to the specimen. The maximum stress was about 183 MPa and the minimum stress was about -30 MPa. The particular spectrum loads applied are given in reference [13] for test M91. The calculated crack-opening stresses plotted in figure 11 show only a small fraction of the number of values computed from the model. The crack-opening stresses follow a very irregular pattern while the cyclic loads are applied; even so, they tend to oscillate about a mean value.

The use of an "equivalent" crack-opening stress concept would greatly reduce the computer times required to complete a simulated test. The use of an equivalent stress is justified, because the crack-opening stresses stabilize under constant-amplitude loading at low to medium stress levels, and they tend to oscillate about a mean value under spectrum loading. The equation used to calculate an equivalent crack-opening stress, $\bar{S}_o$, was

$$\bar{S}_o = \frac{\sum (S_o \, \Delta c)_k}{\sum \Delta c_k} \qquad (7)$$

where the summation was performed over the crack extension increment $c_i + 5\,\rho_{max}$ to $c_i + 10\,\rho_{max}$. The maximum plastic-zone size, ρ_{max}, was calculated using the maximum stress in the spectrum. For extremely high stress levels and low R ratios, where S_o values do not stabilize, the simulated test specimen may fail before the equivalent crack-opening stress routine is activated. The dashed line in figure 11 shows the calculated equivalent crack-opening stress. The predicted crack-growth life using $\bar{S}_o$ was 3.5 percent less than the predicted life using S_o, but the computer time was only about one-half as large (2.6 to 5.6 minutes).

Crack-growth predictions.- The crack-growth rate, at each load cycle, was computed from equation (1), using the current values of S_{max}, S_{min}, and S_o. Equation (1) predicts retardation (or acceleration) if S_o is larger (or smaller) than the crack-opening stress that would have been produced under constant-amplitude loading at S_{max} and S_{min}. To demonstrate how crack-growth rates were calculated under variable-amplitude loading, an example is given. Figure 12 shows a typical variable-amplitude load history. The growth rate was computed from equation (1) using

$$\Delta K_{eff} = \Delta S_{eff_k} \sqrt{\pi c}\ F \tag{8}$$

where ΔS_{eff_k} is the effective stress range on the kth cycle. The growth increment per cycle is

$$\Delta c_k = \left(\frac{dc}{dN}\right)_k \tag{9}$$

(Note that S_o and F are held constant during a small growth increment Δc^*. See the section in appendix A on Crack Extension and Approximations.) On the first and second tensile load excursion, S_{min_k} to S_{max_k},

$$\Delta S_{eff_k} = S_{max_k} - S_o \tag{10}$$

where $k = 1$ or 2, respectively. This equation was proposed by Elber [2]. However, on the third tensile load excursion, S_{min_3} is greater than S_o, therefore the effective stress range was assumed to be

$$\Delta S_{\mathrm{eff}_k} = \left[(S_{\mathrm{max}_k} - S_o)^{C_2} - (S_{\mathrm{min}_k} - S_o)^{C_2}\right]^{\frac{1}{C_2}} \tag{11}$$

where $k = 3$ and C_2 is the power on the growth law. Thus, the growth increment, $\Delta c_2 + \Delta c_3$, is slightly larger than Δc_1, if $S_{\mathrm{max}_1} = S_{\mathrm{max}_3}$. The use of equation (11) was necessary because no crack-growth law, when expressed in terms of a power function ($C_2 \neq 1$), would sum to the correct growth increment under variable-amplitude loading. For instance, if the load excursion S_{max_2} to S_{min_3} was extremely small, then the sum of growth increments Δc_2 and Δc_3 should be equal to the growth increment Δc_1. If S_{min_3} was less than S_o, then the growth increment Δc_3 should be equal to the growth increment Δc. Equation (11) accounts for these limiting behaviors. Equation (11) is applied only when S_{min_k} is greater than S_o and only when the current maximum applied stress is higher than the highest maximum stress occurring since a stress excursion crossed S_o. On the fourth excursion, ΔS_{eff} was, again, computed from equation (10). The effective stress range on the 5th and 7th excursion were, again, computed from equation (11). But on the 6th, 8th, and 9th excusion,

$$\Delta S_{\mathrm{eff}_k} = S_{\mathrm{max}_k} - S_{\mathrm{min}_k} \tag{12}$$

where $k = 6$, 8, or 9, respectively. Note that $S_{\mathrm{max}_6} \leq S_{\mathrm{max}_5}$. Equation (12) was also proposed by Elber [2].

The ASTM E24.06.01 Round Robin involved five basic aircraft-type load spectra applied to center-crack tension specimens. Three of the spectra were each applied at three different scale factors (same shape spectrum with different scaling of the stresses), and the other two spectra were each applied at two different scale factors. There were thirteen different spectrum loading tests. The test specimens were precracked ($S_{max} = 55$ MPa, $R = 0$) from an initial EDM notch ($c_n = 3.18$ mm) to the initial crack lengths given in table 2 before the spectrum loads were applied. See reference [13] for more details.

Figure 13 compares predicted and experimental crack-length-against-cycles curves for a typical fighter spectrum. The specimens were subjected to the same spectrum, but with three different scale factors (0.2, 0.3, and 0.4). The predicted results (curves) are in good agreement with the experimental data (symbols).

Figure 14 compares experimental and predicted lives for the thirteen spectrum loading tests (solid symbols). The predicted results were obtained from the closure model with $\alpha = 2.3$. The ratio of N_P/N_T ranged from 0.66 to 1.48. The mean value of N_P/N_T was 0.98 and standard deviation was 0.28. The results from the constant-amplitude tests (open symbols) are also shown for comparison.

Table 2 shows that the ratio N_P/N_T is lower for higher scale factor tests within each spectrum. This behavior was attributed to the changing constraint at the crack tip. All predictions were made under nearly plane-strain conditions; however, the higher stresses are more likely to produce a plane-stress condition (plastic-zone size is large compared to thickness), especially during a high overload, and, consequently, cause more retardation. These results suggest the need for a variable constaint factor which would be a function of the plastic-zone-to-thickness ratio.

Table 2 also presents the crack-growth predictions submitted to the ASTM E24.06.01 Round Robin [16]. These predictions were made using the analytical closure model but under nearly plane-stress conditions. In the original model, the bar elements were assumed to yield in compression at $-\alpha\sigma_o$, instead of $-\sigma_o$ as is in the present model. This assumption strongly influenced the calculated crack-opening stresses. The crack-growth rate equation was also different from that used herein. The rate equation used in the original model is given in reference [9]. Crack-growth predictions under simulated plane-stress conditions gave higher crack-opening stresses than those under simulated plane-strain conditions (see figs. 8 and 9) and, consequently, retardation effects are much stronger. This may account for the large N_P/N_T ratios obtained on test M88 and M89, where retardation effects dominated.

Table 2 also presents crack-growth predictions using linear-cumulative damage (LCD), that is, no load-interaction effects. The predictions were obtained from Johnson [17]. The predictions are quite good and indicate that retardation and acceleration effects nearly cancel each other for most of the spectra. Only test M88 and M89 had a sufficiently high overload such that retardation effects would dominate the life. Test M93 and M94 were dominated by crack-growth acceleration as is evident from the large N_P/N_T ratios for linear-cumulative damage.

CONCLUDING REMARKS

An analytical fatigue crack-closure model was developed and used in a crack-growth analysis program (FAST) to predict crack growth under constant-amplitude and aircraft spectrum loading. The model was based on the Dugdale model, but modified to leave plastically-deformed material in the wake of the advancing crack tip. The model was used to calculate the crack-opening stresses as a function of crack length and load history under simulated plane-stress and plane-strain conditions.

A crack-growth rate equation was developed in terms of Elber's effective stress-intensity factor range, threshold stress-intensity factor range, and fracture toughness, to give the "sigmoidal" shape commonly observed in fatigue crack-growth rate data plotted against stress-intensity factor range. The five crack-growth constants in this equation were determined from constant-amplitude data on 2219-T851 aluminum alloy sheet material. The equation correlated the constant-amplitude data over a wide range of stress ratios and stress levels quite well.

The analytical closure model, under nearly plane-strain conditions, and the rate equation were used to predict crack growth under aircraft spectrum loading on the 2219-T851 aluminum alloy material. The model predicts the effects of load interaction, such as retardation and acceleration. The ratio of predicted-to-experimental crack-growth lives ranged from 0.66 to 1.48 in thirteen spectrum load tests. However, many of the spectra were not suitable discriminators among load-interaction models because a linear-cumulative damage model made equally good predictions. But these tests did verify whether the models could adequately balance retardation and acceleration effects. The only exceptions to this behavior were tests M88 and M89 where retardation effects dominated, and tests M93 and M94 where acceleration effects dominated. The analytical crack-closure model and the proposed crack-growth law predicted crack growth in all spectrum load tests quite well.

APPENDIX A

GOVERNING EQUATIONS FOR ANALYTICAL CRACK-CLOSURE MODEL

The following sections give the governing equations for the stress and deformation characteristics of the analytical crack-closure model. The sections include a discussion on crack-surface displacements, plastic-zone size, residual plastic deformations, contact stresses, crack-opening stresses, and crack extension.

A schematic of the closure model at maximum and minimum applied stress is shown in figure 3. Because of symmetry, only one quarter of the plate was analyzed. A breakdown on the components of the model and the coordinate system used are shown in figure 15. The plate had a fictitious crack of half-length d and was subjected to a uniform stress S. The rigid-plastic bar element connected to point j was subjected to a compressive stress σ_j. This element is in contact when the length of the element L_j is larger than the current crack-surface displacement V_j. The stress σ_j is applied to make $V_j = L_j$. The equations which govern the response of the complete system were obtained by requiring that compatibility be met between the elastic plate and all of the bar elements along the crack surface and plastic-zone boundary. The displacement at point i is

$$V_i = S\, f(x_i) - \sum_{j=1}^{n} \sigma_j\, g(x_i,x_j) \qquad (13)$$

where $f(x_i)$ and $g(x_i,x_j)$ are influence functions given by

APPENDIX A

$$f(x_i) = \frac{2(1 - \eta^2)}{E} \sqrt{(d^2 - x_i^2) \sec \frac{\pi d}{W}} \tag{14}$$

$$g(x_i, x_j) = G(x_i, x_j) + G(-x_i, x_j) \tag{15}$$

$$G(x_i, x_j) = \frac{2(1 - \eta^2)}{\pi E} \Bigg\{ (b_2 - x_i) \cosh^{-1} \left(\frac{d^2 - b_2 x_i}{d \, |b_2 - x_i|} \right)$$

$$- (b_1 - x_i) \cosh^{-1} \left(\frac{d^2 - b_1 x_i}{d \, |b_1 - x_i|} \right)$$

$$+ \sqrt{d^2 - x_i^2} \left[\sin^{-1} \left(\frac{b_2}{d} \right) - \sin^{-1} \left(\frac{b_1}{d} \right) \right] \Bigg\}$$

$$\left[\frac{\sin^{-1} B_2 - \sin^{-1} B_1}{\sin^{-1}\left(\frac{b_2}{d}\right) - \sin^{-1}\left(\frac{b_1}{d}\right)} \right] \sqrt{\sec\left(\frac{\pi d}{W}\right)} \tag{16}$$

where

$$B_k = \frac{\sin\left(\frac{\pi b_k}{W}\right)}{\sin\left(\frac{\pi \, d}{W}\right)} \quad \text{for} \quad k = 1 \text{ or } 2, \tag{17}$$

$b_1 = x_j - w_j$ and $b_2 = x_j + w_j$. Appendix B explains how these equations were developed. The bar element at point i (not shown in fig. 6) has a length (or residual deformation) of L_i. The compatability equation $(V_i = L_i)$ is expressed as

$$\sum_{j=1}^{n} \sigma_j \, g(x_i, x_j) = S \, f(x_i) - L_i \quad \text{for } i = 1 \text{ to } n \tag{18}$$

subject to various constraints. One type of constraint is caused by tensile or compressive yielding of the bar elements and the other is caused by element separation $(V_i \geq L_i)$ along the crack surface. The method used to solve equations (18) subject to the constraints is described in appendix D.

Plastic-Zone Size and Approximations

The plastic-zone size, ρ, for a crack in a finite-width specimen, was determined by requiring that the finiteness condition of Dugdale be satisfied. This condition states that the stress-intensity factor at the tip of the plastic zone is zero and is given by

$$(K)_S + (K)_{\sigma_o} = 0 \tag{19}$$

where

$$(K)_S = S_{max} \sqrt{\pi d \sec\left(\frac{\pi d}{W}\right)} \tag{20}$$

and

$$(K)_{\sigma_o} = -\alpha\sigma_o \left\{1 - \frac{2}{\pi} \sin^{-1} \left[\frac{\sin \frac{\pi c}{W}}{\sin \frac{\pi d}{W}}\right]\right\} \sqrt{\pi d \sec\left(\frac{\pi d}{W}\right)} \tag{21}$$

Equations (20) and (21) are discussed in appendix B. Solving equation (19) for d, and noting that $\rho = d - c$, gives

$$\rho = c \left\{\frac{W}{\pi c} \sin^{-1} \left[\sin\left(\frac{\pi c}{W}\right) \sec\left(\frac{\pi S_{max}}{2\, \alpha\sigma_o}\right)\right] - 1\right\} \tag{22}$$

For $\alpha = 1$, equation (22) reduces to the expression derived by Rice [18].

In the model, the plastic zone was arbitrarily divided into ten graduated bar elements. The aspect ratios, $2w_i/\rho$, were 0.01, 0.01, 0.02, 0.04, 0.06, 0.09, 0.12, 0.15, 0.2, and 0.3. The smallest elements were located near the crack tip $(x = c)$. Doubling the number of elements in the plastic zone had less than a 1 percent effect on claculated crack-opening stresses. At the maximum applied stress, the plastic-zone size was calculated from equation (22). The length, L_i, of the bar elements in the plastic zone were calculated from equation (13) as

$$L_i = V_i = S_{max}\, f(x_i) - \sum_{j=1}^{10} \alpha\sigma_o\, g(x_i,x_j) \tag{23}$$

APPENDIX A

where $f(x_i)$ and $g(x_i,x_j)$ are given by equations (14) and (15), respectively. The bar elements act as rigid wedges. The plastic deformation (L_i) changes only when an element yields in tension ($\sigma_j \geq \alpha\sigma_o$) or compression ($\sigma_j \leq -\sigma_o$). The constraint factor was assumed to apply only during tensile loading. Figure 3(a) shows a schematic of the model at the maximum applied stress. Here the crack surfaces are fully open and the residual deformations do not affect the crack-surface displacements.

The division of the plastic zone into a number of finite elements would allow for the eventual use of a nonlinear stress-strain curve with kinematic hardening instead of the rigid-perfectly plastic assumptions used herein. This may give a more realistic crack-closure behavior. The models developed in references [7], [8], [10], and [11] are not well suited for incorporating a nonlinear stress-strain curve.

Contact Stresses at Minimum Load

When the analytical closure model is unloaded to the minimum load (fig. 3(b)), the bar elements in the plastic zone unload until some of the elements near the crack tip yield in compression ($\sigma_j \leq -\sigma_o$). The compressive plastic zone, ω, is shown as the shaded region at the crack tip. Depending upon the amount of closure and constraint factor, ω varies from one-tenth to one-half of the plastic zone ρ. The original cyclic Dugdale model (no closure) [18] predicts that ω equals $0.25\ \rho$ at $R = 0$ and $\alpha = 1$. Thus, crack closure greatly affects the size of the compressive plastic zone. The elements along the crack surfaces, which store the residual deformations, may come into contact and carry compressive stresses. Some of these elements may also yield in compression ($\sigma_j \leq -\sigma_o$). The stresses in the plastic zone and the contact stresses along the crack surfaces are calculated from equations (18) with $S = S_{min}$. For elements that yield in compression, σ_i is set equal to $-\sigma_o$ and the lengths of the elements are set equal to the final displacements at those points. That is,

$$L_i = V_i - S_{min} f(x_i) - \sum_{j=1}^{n} \sigma_j g(x_i, x_j) \qquad (24)$$

For elements not in contact $(L_i < V_i)$, $\sigma_i = 0$.

Crack-Opening Stresses

The applied stress level at which the crack surfaces are fully open (no surface contact) denoted as S_o, was calculated from the contact stresses at S_{min}. To have no surface contact, the stress-intensity factor due to an applied stress increment $(S_o - S_{min})$ is set equal to the stress-intensity factor due to the contact stresses. Solving for S_o gives

$$S_o = S_{min} - \sum_{j=11}^{n-1} \frac{2\sigma_j}{\pi} [\sin^{-1} B_2 - \sin^{-1} B_1] \qquad (25)$$

where

$$B_k = \frac{\sin\left(\frac{\pi b_k}{W}\right)}{\sin\left(\frac{\pi c_o}{W}\right)} \quad \text{for } k = 1 \text{ or } 2, \tag{26}$$

and c_o is the current crack length minus Δc^*. The increment Δc^* is the width of element n, and its significance is discussed in the next section. If $\sigma_j = 0$ for $j = 11$ to $n - 1$ at the minimum applied stress, then the crack is already fully open, and S_o cannot be determined from equation (25). The stress σ_j at the crack tip changes from compression to tension when the applied stress level reaches S_o.

Crack Extension and Approximations

The analytical closure model provides no information about the amount of crack growth per cycle. Crack growth is simulated by extending the crack an incremental value at the moment of maximum applied stress. The amount of crack extension, Δc^*, was arbitrarily defined as

$$\Delta c^* = 0.05\ \rho_{max} \tag{27}$$

where ρ_{max} is the plastic-zone size caused by the maximum applied stress occurring during the Δc^* growth increment. The number of load cycles, ΔN, required to grow the crack an increment Δc^* was calculated from equation (1) and the cyclic load history. Typical values of Δc^* ranged between 0.004 mm to 0.1 mm, depending upon the applied stress level and crack length. The coefficient (0.05) was selected after a systematic study was made on the effects of the size of Δc^* on crack-opening stresses and on computer time. Smaller values of Δc^* increase the computer time. The choice of the coefficient in this range did not adversely affect the crack opening stresses under constant-amplitude loading but some sequence effects were lost under variable-amplitude loading.

The resulting computer times were considered reasonable. Under constant-amplitude loading, a simulated fatigue-crack growth test, from the initial crack length to failure, required 0.5 to 5 minutes on a CDC-6600 computer. Under spectrum loading, a simulated test to failure required from 2 to 15 minutes. The computer storage requirements for the analytical closure model and crack-growth program was low (less than 70K). The larger computer times occurred on tests that were conducted at low stress levels and high R ratios. But these computer times could be drastically reduced if an "equivalent" crack-opening stress were used in the latter stage of a simulated test. The use of an equivalent crack-opening stress is justified because crack-opening stresses stabilize very quickly under low stress levels and high R ratios. The equivalent crack-opening stress is discussed in the section on "Application of the Crack-Closure Model and Rate Equation."

The simulated crack extension Δc^* creates a new bar element at the crack tip. The length of the new element is equal to the displacement at the crack tip before the crack extends.

The calculated crack-opening stresses and the boundary-correction factors were held constant while the crack was grown under cyclic loading (cycle-by-cycle) over the length Δc^*. The number of load cycles, ΔN, required to grow

APPENDIX A

the crack an increment Δc^* was calculated from equation (1) and the cyclic load history. When the sum of the crack growth increments (Δc) equalled or exceeded Δc^*, the analytical closure model was exercised. If ΔN reached 300 cycles, the model was exercised whether or not Δc^* was reached. This limits the number of cycles that can be applied before the model is exercised. The increment Δc^* was set equal to summation of Δc's. Thus, Δc^* was less than or equal to that computed from equation (27) and the number of cycles ranged from 1 to 300. During the cyclic growth computations, the cyclic stress history was monitored to find the lowest applied stress before (S_{min_b}) and after (S_{min_a}) the highest applied stress level (S_{max_h}). The application of the analytical closure model consisted of:

1. Applying minimum stress S_{min_b} at crack length c.
2. Applying maximum stress S_{max_h} at crack length c.
3. Extending crack an increment Δc^*.
4. Applying minimum stress S_{min_a} at crack length $c + \Delta c^*$.
5. Calculating new crack-opening stress S_o from equation (25).
6. Continuing cyclic load history.
7. Calculating new Δc^* from equation (27).
8. Repeating process when crack extension reaches new Δc^* or ΔN reaches 300 cycles.

Steps 1 through 4 require solving equations (18) for the contact stresses and the stresses in the plastic zone. The overall procedure is repeated until the desired crack length is reached or the specimen fails. The failure criterion used to terminate the simulated test is discussed in appendix C.

APPENDIX A

To keep the number of elements to a reasonable size (20 to 30), a "lumping" procedure was used. The lumping procedure combines adjacent elements (i and $i + 1$) together to form a single element if

$$2(w_i + w_{i+1}) \leq c - x_{i+1} + \Delta c^* \tag{28}$$

Thus, elements near the crack tip are not as likely to be lumped together as those that are away from the crack tip. In the lumping procedure, the width of the lumped element was the sum of the widths for the two adjacent elements and the length was the weighted average of the two:

$$L = \frac{L_i w_i + L_{i+1} w_{i+1}}{w_i + w_{i+1}} \tag{29}$$

APPENDIX B

EQUATIONS FOR STRESS-INTENSITY FACTORS AND CRACK-SURFACE DISPLACEMENTS

The equations for stress-intensity factors and crack-surface displacements for a crack in an infinite plate were obtained from the literature [19]. These equations are modified herein for finite plates. Some of the approximate equations for finite plates were verified with boundary-collocation analyses [20].

Stress-Intensity Factors for a Crack in an Infinite Plate

The stress-intensity factors for the configurations shown in figure 2, with W equal to infinity, were obtained from reference [19].

Remote uniform stress.- The stress-intensity factor for a crack in an infinite plate is

$$K_\infty = S \sqrt{\pi d} \tag{30}$$

Partially-loaded crack.- The stress-intensity factor for the configuration shown in figure 2(b) is

$$K_\infty = \frac{2\sigma}{\pi} \sqrt{\pi d} \left[\sin^{-1}\left(\frac{b_2}{d}\right) - \sin^{-1}\left(\frac{b_1}{d}\right)\right] \tag{31}$$

APPENDIX B

Crack-Surface Displacements for a Crack in an Infinite Plate

The crack-surface displacements for the configurations shown in figure 4, again, with W equal to infinity were obtained from Westergaard stress functions given in reference [19]. The following sections give the displacement equations for remote uniform stress and the partially-loaded crack.

Remote uniform stress.- The crack-opening displacements for the configuration shown in figure 2(a) with $W = \infty$ is

$$V_\infty = \frac{2\,(1 - \eta^2)\,S}{E} \sqrt{d^2 - x^2} \tag{32}$$

for $|x| \leq d$, where $\eta = \nu$ for plane strain and $\eta = 0$ for plane stress.

Partially-loaded crack.- The crack-opening displacements for the configuration shown in figure 2(b) with $W = \infty$ is

$$V_\infty = V(x) + V(-x) \tag{33}$$

where

$$V(x) = \frac{2\,(1 - \eta^2)}{\pi E} \left[(b - x) \cosh^{-1} \left(\frac{d^2 - bx}{d\,|b - x|} \right) + \sqrt{d^2 - x^2} \quad \sin^{-1} \left(\frac{b}{d} \right) \right] \Bigg|_{b=b_1}^{b=b_2} \quad \text{for } |x| \leq d. \tag{34}$$

APPENDIX B

Finite-Width Corrections

The equations given in the preceding sections for the stress-intensity factors and crack-surface displacements (eqs. (30) to (34)) were for a crack in an infinite plate. But these quantities are influenced by the finite width of the plate. Because there are no closed form solutions for finite-width specimens, approximate equations are developed herein. The stress-intensity factor for a crack in a finite-width plate is

$$K = K_\infty F \tag{35}$$

where F is the finite-width correction for the particular loading condition. Noting that the elastic crack-surface displacements in the region of the crack tip are directly related to the stress-intensity factor, it is proposed that the same correction factor be used for displacements:

$$V = V_\infty \left(\frac{K}{K_\infty}\right) = V_\infty F \tag{36}$$

where V is the displacement for a crack in a finite-width plate subjected to the particular loading condition. Equation (36) gives very accurate crack-surface displacements in the region near the crack tip, as expected.

<u>Remote uniform stress</u>.- The approximate boundary-correction factor for a central crack in a finite-width plate subjected to uniform stress [19,21] as shown in figure 2(a) is

APPENDIX B

$$F = \sqrt{\sec\left(\frac{\pi d}{W}\right)} \tag{37}$$

The crack-surface displacements, V, given by equations (32), (36), and (37) were compared with calculated displacements from reference [20], which used the boundary-collocation method, and the results were found to be within 2 percent of each other for any value of x for $2d/W \leq 0.7$. The crack-surface displacements near the crack tip were very accurate, as expected.

Partially-loaded crack.- The approximate boundary-correction factor for a central crack in a finite-width plate subjected to partial loading on the crack surface (fig. 2(b)) was obtained from the infinite periodic array of cracks solution [19] and was modified herein by replacing the term $W/\pi d \tan(\pi d/W)$ by $\sec(\pi d/W)$. It was shown in reference [21] that the "secent" term gave more accurate results for stress intensity than the "tangent" term. The resulting boundary-correction factor was

$$F = \left[\frac{\sin^{-1} B_2 - \sin^{-1} B_1}{\sin^{-1}\left(\frac{b_2}{d}\right) - \sin^{-1}\left(\frac{b_1}{d}\right)}\right] \sqrt{\sec \frac{\pi d}{W}} \tag{38}$$

where

$$B_i = \frac{\sin\left(\frac{\pi b_i}{W}\right)}{\sin\left(\frac{\pi d}{W}\right)} \tag{39}$$

When $b_1 = 0$ and $b_2 = d$ (uniformly-stressed crack surface), equation (38) reduces to equation (37), as expected.

APPENDIX C

FAILURE CRITERION

The failure criterion used to terminate the simulated fatigue-crack growth tests was the Two-Parameter Fracture Criterion (TPFC) [15]. The criterion involves two fracture parameters, K_F and m, that are determined from the fracture data. Because no fracture data were reported in reference [13], the final crack lengths (recorded) and the maximum stress levels in the fatigue-crack growth tests (constant-amplitude, variable-amplitude and spectrum loading) were used to estimate the fracture parameters, K_F and m. Figure 16 shows a plot of the elastic stress-intensity factors at failure, K_{Ie}, against the maximum applied fatigue stress level. At a given stress level, the large amount of variation was attributed to the final crack lengths reported being less than the critical values and the maximum stress levels in the variable-amplitude and spectrum loading tests were larger than the actual failure stresses. The fracture parameter, m, was taken as unity because fracture data on 2219-T851 aluminum alloy in reference [15] showed that m was unity for specimen thicknesses less than 25 mm. The specimen thickness in reference [13] was 6.35 mm. The elastic-plastic fracture toughness, K_F, was chosen to be 550 MPa-$m^{1/2}$ to fit the upper bound for most of the test data. The solid curve in figure 16 shows the calculated K_{Ie} values at failure from the TPFC for the center-crack tension specimens (W = 152.4 mm) used in reference [13]. These results indicate that specimens tested at low stress levels fail at lower stress-intensity factors than those tested at higher stress levels.

APPENDIX C

The maximum value of K_{Ie} from the solid curve was about 77 MPa-m$^{1/2}$. This is the value of the coefficient C_5 used in equation (1).

APPENDIX D

GAUSS-SEIDEL ITERATIVE METHOD WITH CONSTRAINTS

The method used to solve the linear system of equations (eqs. (18)) is the Gauss-Seidel iterative method [22] with constraints added. This method was chosen because the number of equations to be solved were variable (10 to 40). The constraints are of two types. One type is caused by yielding (tensile or compressive) of the bar elements; the other is caused by element separation along the crack surface. The equations, which govern the deformations along the crack surface and in the plastic zone, are

$$\sum_{j=1}^{n} \sigma_j \, g(x_i,x_j) = S \, f(x_i) - L_i \tag{40}$$

where S is the current applied stress, L_i is the residual plastic deformation for element i, n is the number of elements, and σ_j are the contact stresses along the crack surfaces and the stresses in the plastic zone. Equations (40) are solved with the following constraints:

For elements in the plastic-zone region $(x_j > c)$,

$$\text{if} \qquad \sigma_j > \alpha\sigma_o \quad \text{set} \quad \sigma_j = \alpha\sigma_o \tag{41}$$

APPENDIX D

if $\sigma_j < -\sigma_o$ set $\sigma_j = -\sigma_o$ (42)

These constraints are for tensile and compressive yielding, respectively. For elements along the crack surfaces $(x_j \leq c)$,

if $\sigma_j > 0$ set $\sigma_j = 0$ (43)

if $\sigma_j < -\sigma_o$ set $\sigma_j = -\sigma_o$ (44)

These constraints are for element separation and compressive yielding, respectively.

First, rewriting equations (4) in the form

$$\sum_{j=1}^{n} \sigma_j \, g_{ij} = S \, f_i - L_i \tag{45}$$

and solving for σ_i gives

APPENDIX D

$$\sigma_i = (S\ f_i - L_i - \sum_{\substack{j=1 \\ j\neq i}}^{n} \sigma_j\ g_{ij})/g_{ii} \tag{46}$$

for i = 1,2,...,n. The matrix, g_{ij} is diagonally dominant, that is, each diagonal coefficient g_{ii} is larger, in absolute value, than the magnitudes of other entries in row i and column i. Next, make initial guesses for σ_i and insert these into the right-hand side of equations (46). If the initial guesses for σ_i are zero, the resulting new approximations are

$$\left.\begin{aligned}
(\sigma_1)_1 &= [S\ f_1 - L_1]/g_{11} \\
(\sigma_2)_1 &= [S\ f_2 - L_2 - (\sigma_1)_1\ g_{21}]/g_{22} \\
&\ \ \vdots \\
(\sigma_n)_1 &= [S\ f_n - L_n - \sum_{\substack{j=1 \\ j\neq n}}^{n} (\sigma_j)_1\ g_{nj}]/g_{nn}
\end{aligned}\right\} \tag{47}$$

The additional subscript on σ_i denotes the iteration number. The stresses $(\sigma_i)_1$ are checked against the constraint equations (41) through (44), as soon as they are computed, and are updated, if necessary. Note that the newly-computed values of σ_i are always used in the right-hand sides as soon as they are obtained. Resubstituting $(\sigma_i)_1$ into the right-hand sides of equations (46), subject to the constraint equations, gives σ_i for the next iteration. This process is repeated until the changes in σ_i are less than some small preset value $(0.02\ \sigma_o)$. The recurrence equation is

$$(\sigma_i)_I = \left[S\ f_i - L_i - \sum_{j=1}^{i-1} (\sigma_j)_I\ g_{ij} - \sum_{j=i+1}^{n} (\sigma_j)_{I-1}\ g_{ij} \right] / g_{ii} \tag{48}$$

where I is the current iteration number. Typically, the number of elements (n) ranged from 10 to 35 and the iterations ranged from 2 to 15.

REFERENCES

1. Elber, W.: Fatigue Crack Closure Under Cyclic Tension, Engineering Fracture Mechanics, Vol. 2, No. 1, July 1970, pp. 37-45.

2. Elber, W.: The Significance of Fatigue Crack Closure, ASTM STP-486, American Society for Testing and Materials, 1971, pp. 230-242.

3. Newman, J. C., Jr.: Finite-Element Analysis of Fatigue Crack Propagation - Including the Effects of Crack Closure, Ph.D. Thesis, VPI&SU, Blacksburg, VA, May 1974.

4. Newman, J. C., Jr.; and Armen, Harry, Jr.: Elastic-Plastic Analysis of a Propagating Crack Under Cyclic Loading, AIAA Journal, Vol. 13, No. 8, August 1975, pp. 1017-1023.

5. Obji, K.; Ogura, K.; and Ohkubo, Y.: Cyclic Analysis of a Propagating Crack and Its Correlation with Fatigue Crack Growth, Engineering Fracture Mechanics J., Vol. 7, 1975, pp. 457-464.

6. Newman, J. C., Jr.: A Finite-Element Analysis of Fatigue-Crack Closure, Mechanics of Crack Growth, ASTM STP-590, American Society for Testing and Materials, 1976, pp. 281-301.

7. Dill, H. D.; and Saff, C. R.: Spectrum Crack Growth Prediction Method Based on Crack Surface Displacement and Contact Analyses, Fatigue Crack Growth Under Spectrum Loads, ASTM STP-595, American Society for Testing and Materials, 1976, pp. 306-319.

8. Budiansky, B.; and Hutchinson, J. W.: Analysis of Closure in Fatigue Crack Growth, Division of Applied Science, DAS M-1, Harvard University, June 1977.

9. Hardrath, H. F.; Newman, J. C., Jr.; Elber, W.; and Poe, C. C., Jr.: Recent Developments in Analysis of Crack Propagation and Fracture of Practical Materials, Fracture Mechanics, edited by N. Perrone, University Press of Virginia, 1978.

10. Führing, H.; and Seeger, T.: Dugdale Crack Closure Analysis of Fatigue Cracks Under Constant Amplitude Loading, Engineering Fracture Mechanics J., Vol. 11, 1979, pp. 99-122.

11. Führing, H.; and Seeger, T.: Structural Memory of Cracked Components Under Irregular Loading, Fracture Mechanics, ASTM STP-677, C. W. Smith, Ed., American Society for Testing and Materials, 1979, pp. 144-167.

12. Dugdale, D. S.: Yielding of Steel Sheets Containing Slits, Journal Mech. Phys. Solids, Vol. 8, 1960.

13. Chang, J. B.; and Stolpestad, J. H.: Improved Methods for Predicting Spectrum Loading Effects - Phase I Report, AFFDL-TR-79-3036, Volume II, March 1978.

14. Hudak, S. J.; Saxena, A.; Bucci, R. J.; and Malcolm, R. C.: Development of Standard Methods of Testing and Analyzing Fatigue Crack Growth Rate Data, AFML-TR-78-40, May 1978.

15. Newman, J. C., Jr.: Fracture Analysis of Various Cracked Configurations in Sheet and Plate Materials, Properties Related to Fracture Toughness, ASTM STP-605, American Society for Testing and Materials, 1976, pp. 104-123.

16. Chang, J. B.: Round Robin Crack Growth Predictions on Center Crack Tension Specimens Under Random Spectrum Loading, Methods and Models for Predicting Crack Growth Under Random Loading, ASTM STP, 1981.

17. Johnson, W. S.: Multi-Parameter Yield Zone Model for Predicting Spectrum Crack Growth. Methods and Models for Predicting Fatigue Crack Growth Under Random Loading, ASTM STP, 1981.

18. Rice, J. R.: The Mechanics of Crack Tip Deformations and Extension by Fatigue, Brown University Tech. Report, NSF GK-28613, May 1966.

19. Tada, H.; Paris, P. C.; and Irwin, G. R.: The Stress Analysis of Cracks Handbook, Del Research Corporation, 1973.

20. Newman, J. C., Jr.: Crack-Opening Displacements in Center-Crack, Compact, and Crack-Line Wedge-Loaded Specimens, NASA TN D-8268, 1976.

21. Brown, W. F., Jr.; and Srawley, J. D.: Plane Strain Crack Toughness Testing of High Strength Metallic Materials, ASTM STP-410, American Society for Testing and Materials, 1969, p. 79.

22. Carnahan, B.; Luther, A. H.; and Wilkes, J. O.: Applied Numerical Methods, John Wiley and Sons, New York, 1969.

TABLE 1.- COMPARISON OF EXPERIMENTAL AND PREDICTED CRACK GROWTH LIVES UNDER CONSTANT-AMPLITUDE LOADING

S_{max}, MPa	R	c_i, mm	c_f, mm	Test N_T Cycles	Closure Model $\frac{N_P}{N_T}$ (α = 2.3)
55	-1.0	4.89	24.6	129,239	1.42
55	-0.3	3.87	17.6	144,000	1.71(a,b)
55	-0.1	3.91	18.7	175,000	1.49
55	0.0	3.55	52.4	352,406	0.98
55	0.3	3.87	6.9	245,000	0.84
138	-0.3	4.13	45.7	9,950	1.04
138	-0.1	3.85	43.0	12,706	0.96
138	0.01	3.87	50.0	13,300	0.98
138	0.01	4.00	42.0	12,180	1.03
138	0.01	6.67	38.3	7,856	0.93
138	0.2	4.57	48.0	11,175	1.19
138	0.3	4.06	43.6	22,950	0.80
138	0.7	3.94	12.1	158,700	0.87
276	-0.3	4.06	21.9	251	2.09(b)
276	-0.1	3.94	21.4	469	1.12
276	0.01	3.83	14.9	846	0.83
276	0.3	3.94	12.9	1,693	0.64
276	0.7	3.94	23.5	14,870	0.89

(a) This test is suspect based on other tests in reference 13.

(b) These tests were not used in obtaining crack-growth constants.

TABLE 2.- COMPARISON OF EXPERIMENTAL AND PREDICTED CRACK GROWTH LIVES UNDER SPECTRUM LOADING

SPECTRUM TYPE	SCALE FACTOR	SPECIMEN	c_i, mm	c_f, mm	Test N_T Cycles	Closure Model		LCD$^{(b)}$ [17]
						$\alpha = 2.3$ $\frac{N_P}{N_T}$	(a) $\frac{N_P}{N_T}$	$\frac{N_P}{N_T}$
Air-to-Air Fighter	0.2 0.3 0.4	M81 M82 M83	4.06 3.81 3.81	13.0 35.4 23.3	115,700 58,585 18,612	1.20 0.71 0.66	1.01 0.67 0.64	1.27 0.85 0.89
Air-to-Ground Fighter	0.2 0.3 0.4	M84 M85 M86	4.00 3.66 3.87	55.9 44.1 32.8	268,908 95,642 36,397	1.48 0.96 0.72	1.47 0.89 0.65	1.09 0.81 0.70
Navigation Fighter	0.3 0.4	M88 M89	3.81 3.81	45.8 38.4	380,443 164,738	1.47 1.06	2.52 1.47	0.73 0.62
Composite Mission Fighter	0.2 0.3 0.4	M90 M91 M92	3.87 3.81 3.81	51.6 36.1 29.5	218,151 65,627 22,187	1.14 0.85 0.74	1.17 0.78 0.69	1.09 0.87 0.88
Composite Mission Transport	0.2 0.3	M93 M94	6.35 6.54	13.6 9.5	1,354,024 279,000	1.02 0.76	0.76 1.25	3.00 1.81
					Mean Std Dev	0.98 0.28	1.12 0.50	1.12 0.63

(a) Predictions submitted in ASTM E24.06.01 Round Robin.

(b) Linear-cumulative damage (no retardation and no acceleration) predictions from reference 17.

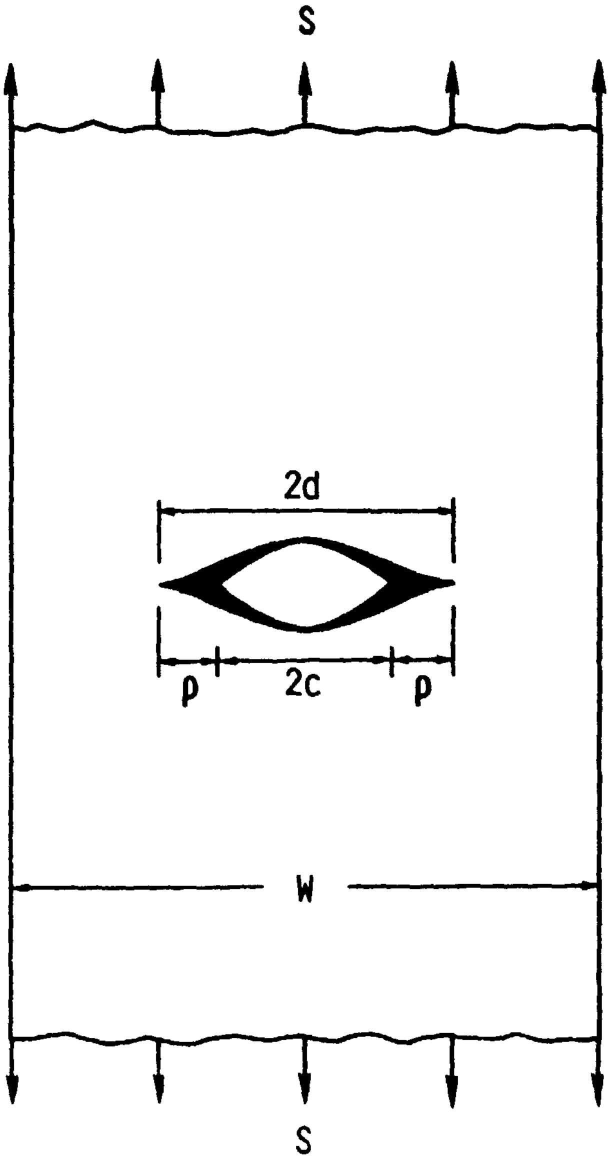

FIG. 1 - Center-crack tension specimen with Dugdale plastic zones and residual plastic deformations.

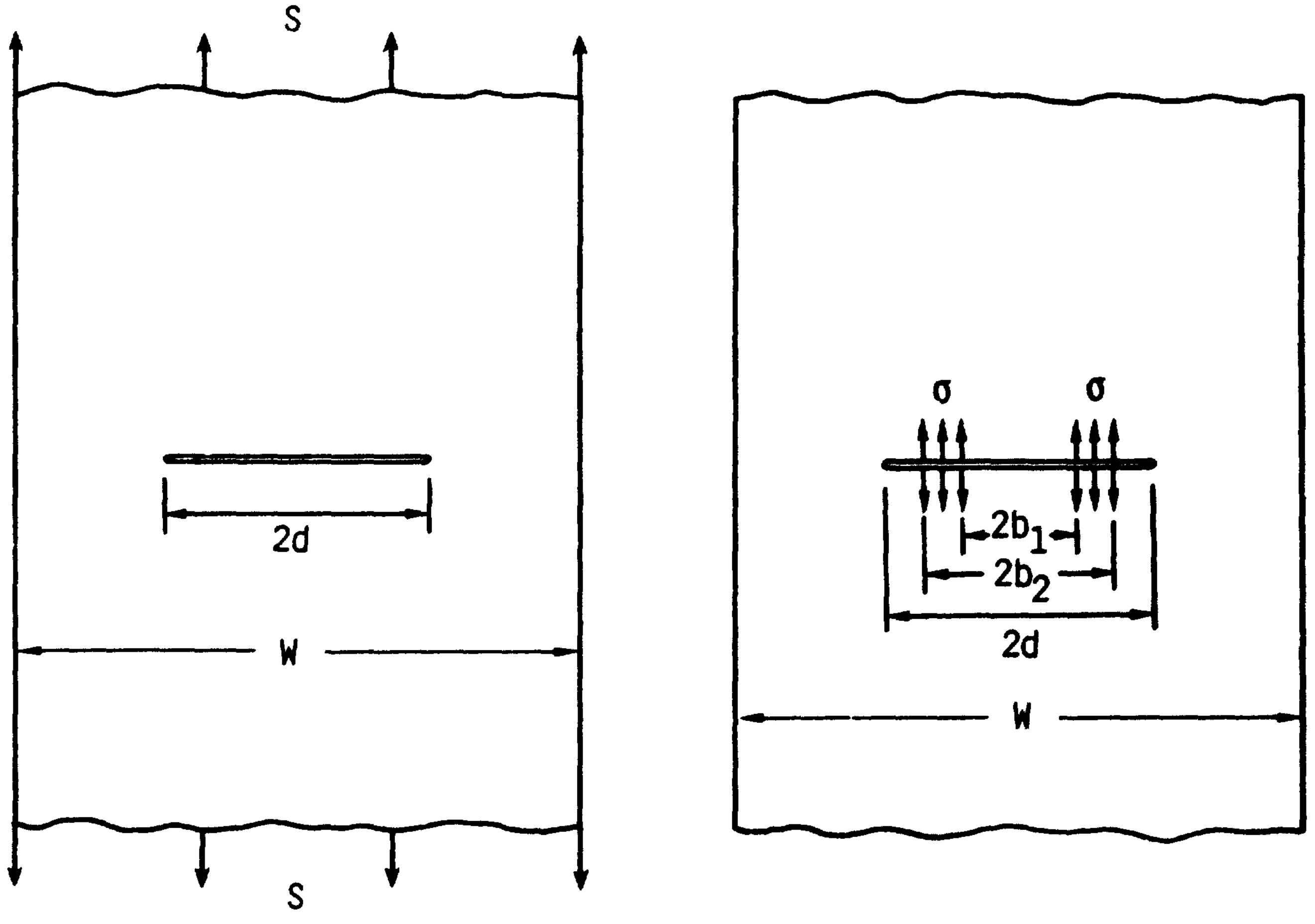

(a) Uniform stress

(b) Partially-loaded crack

FIG. 2 - Crack in a finite-width elastic plate subjected to various loading.

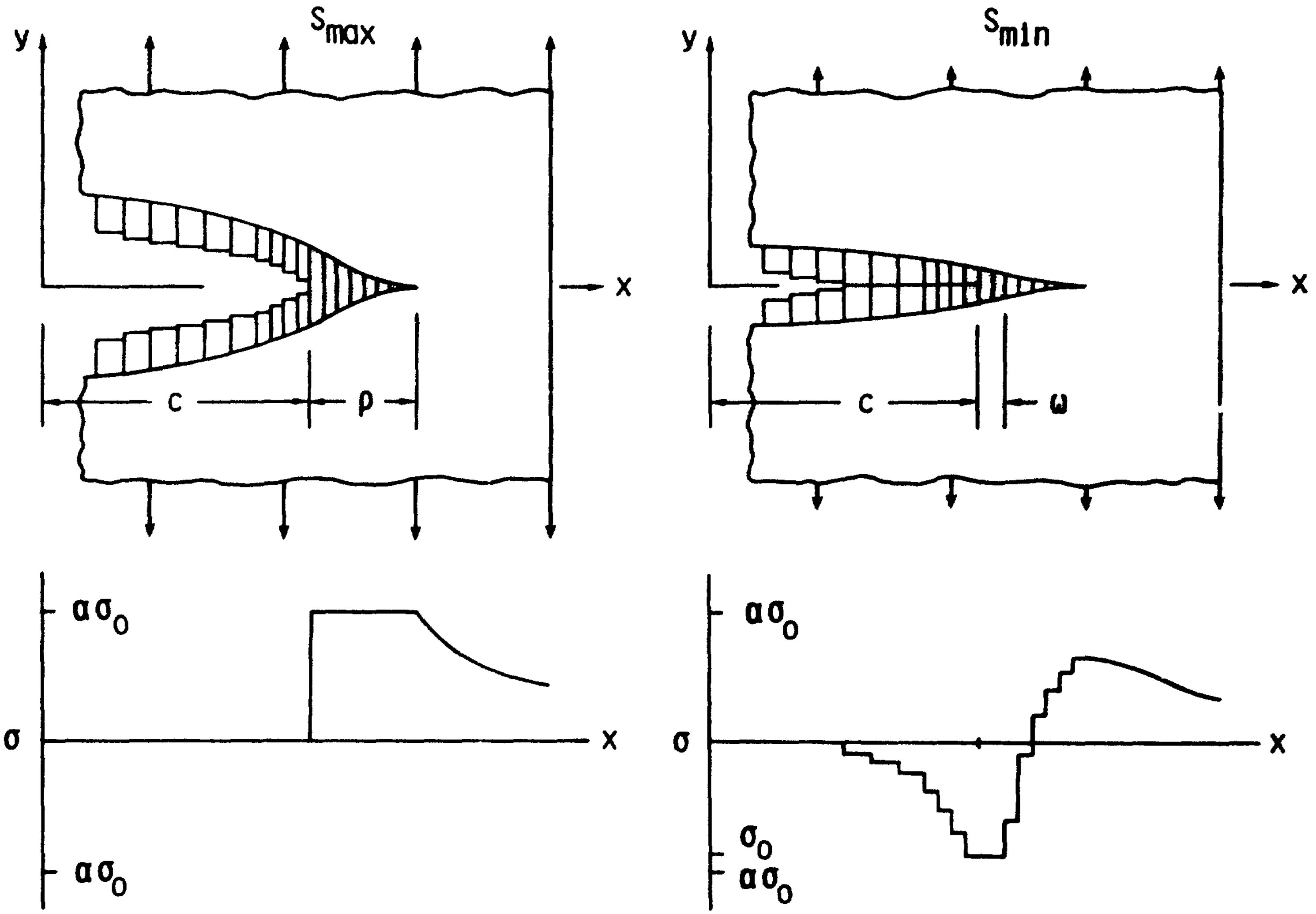

(a) Maximum stress

(b) Minimum stress

FIG. 3 - Crack-surface displacements and stress distributions along crack line.

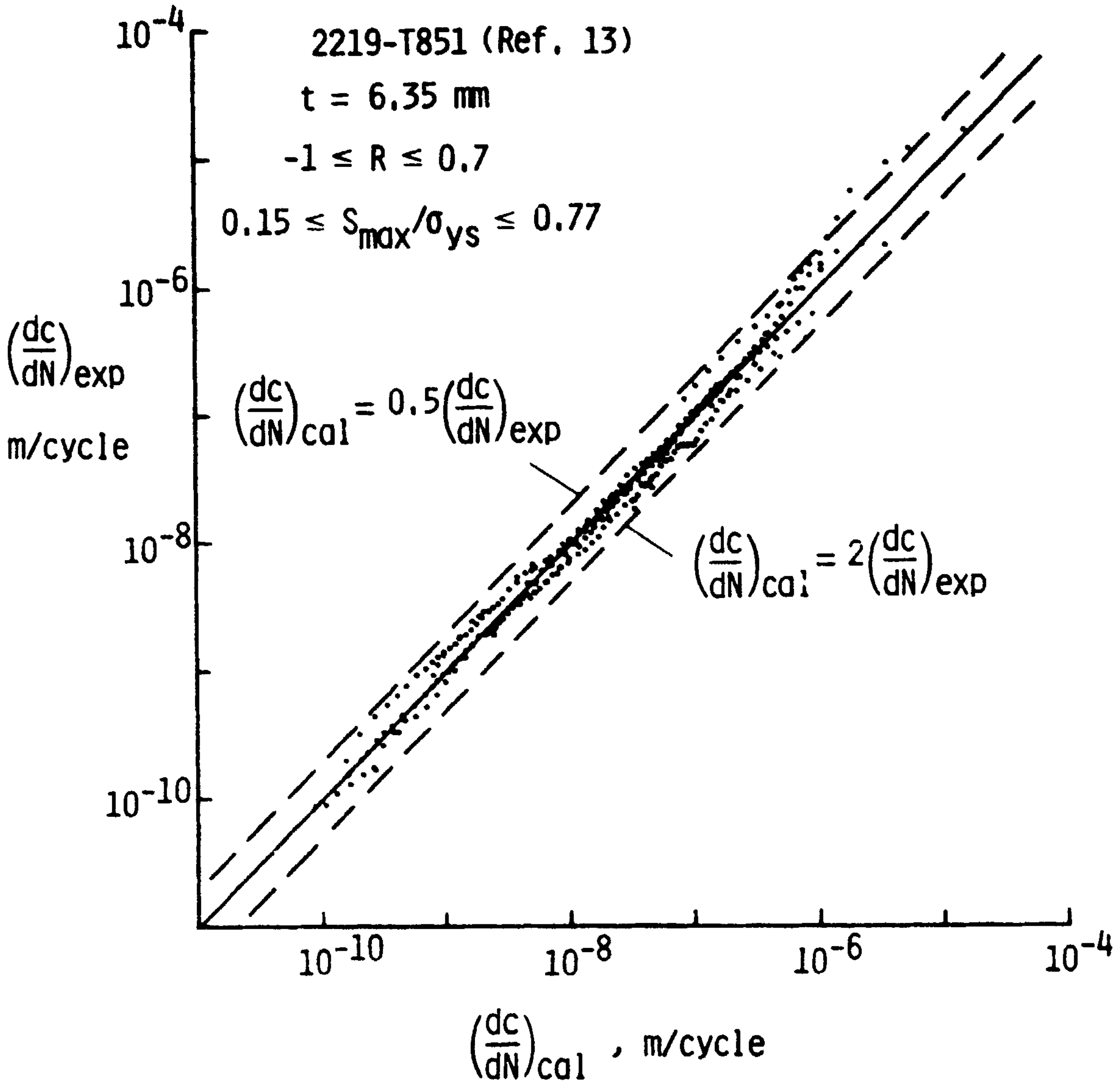

FIG. 4 - Comparison of experimental and calculated crack-growth rates for 2219-T851 aluminum alloy.

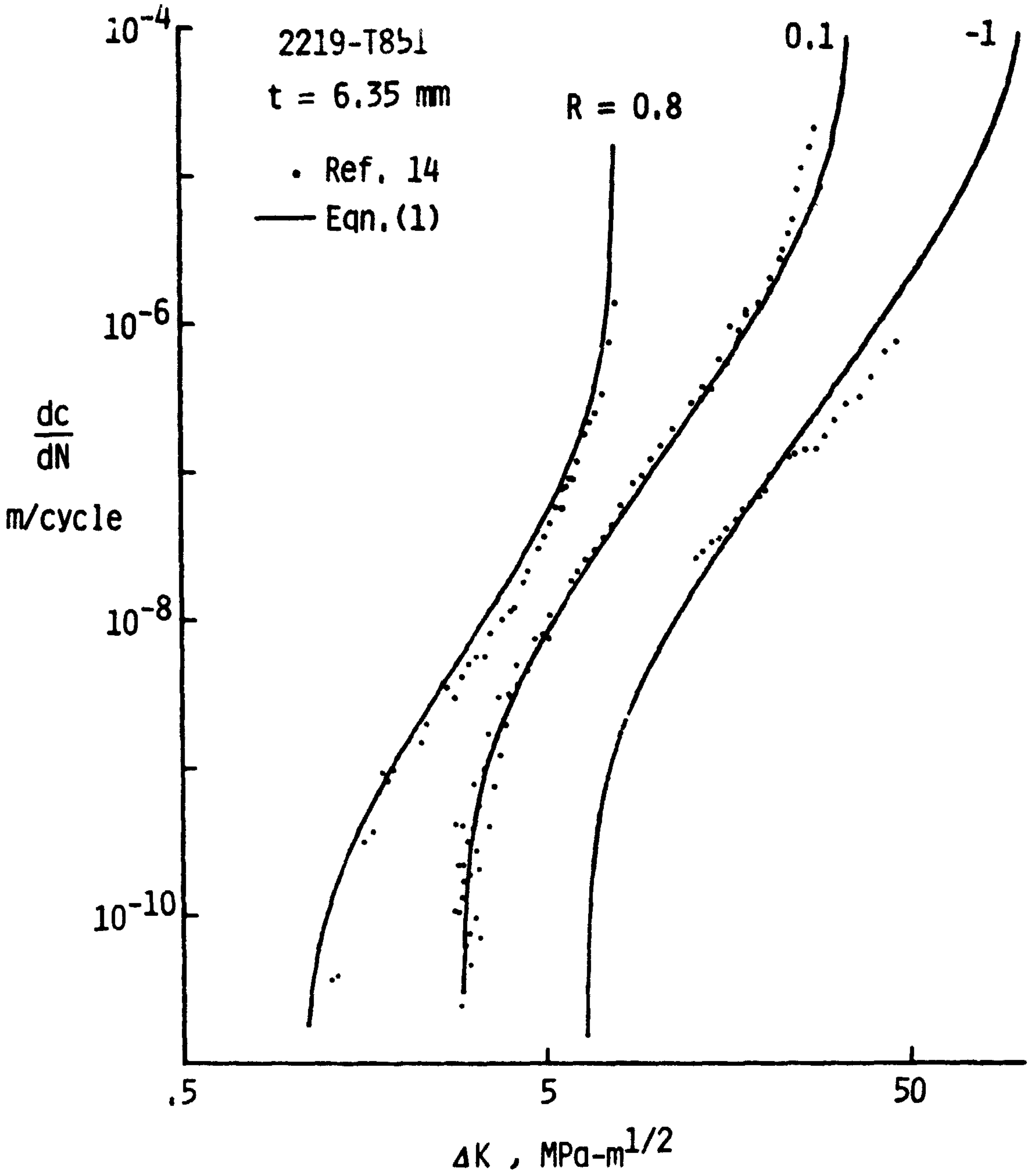

FIG. 5 - Comparison of experimental crack-growth rates and rate equation for 2219-T851 aluminum alloy at various R ratios.

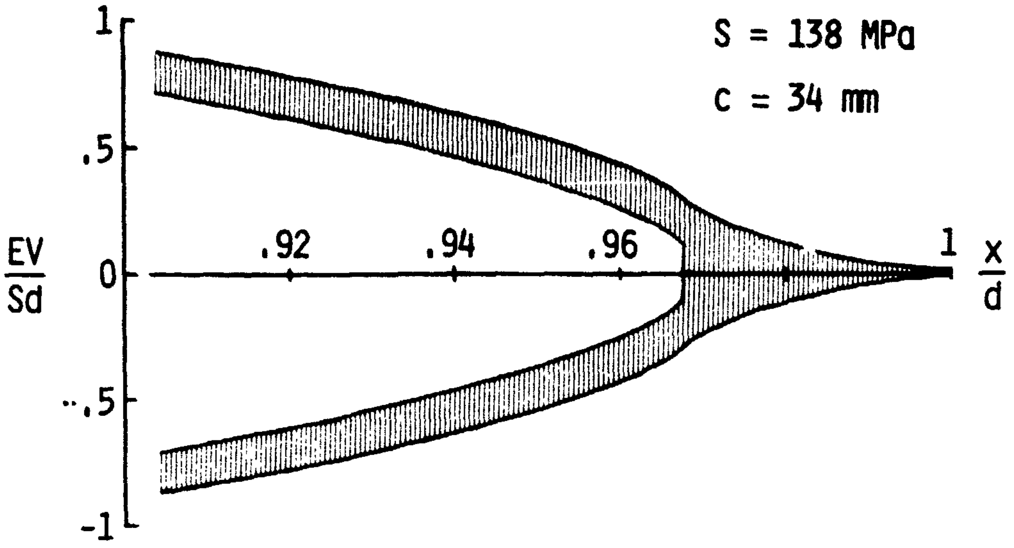

(a) Displacement profile at maximum load

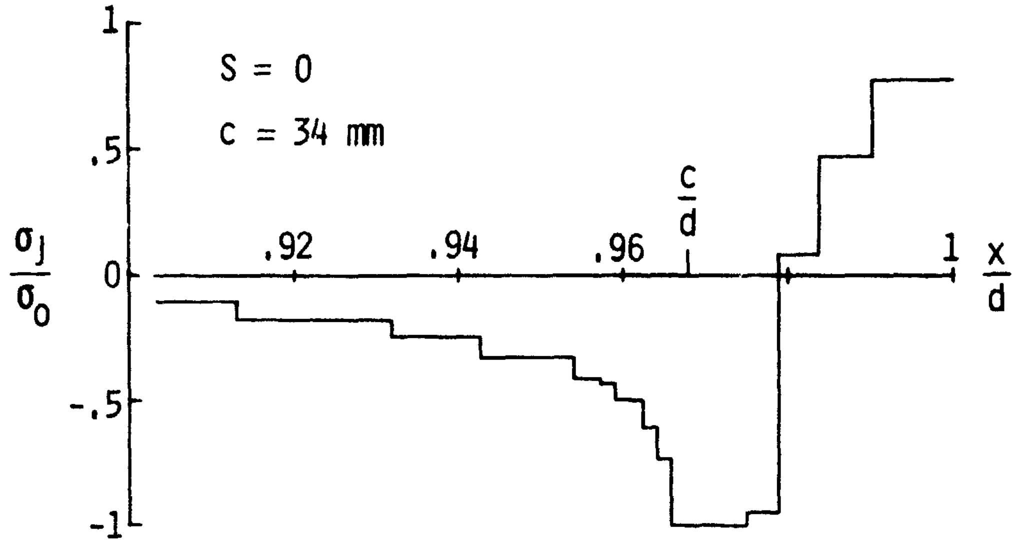

(b) Contact stresses at minimum load

FIG. 6 - Crack-surface displacements and contact stresses under constant-amplitude loading (R = 0).

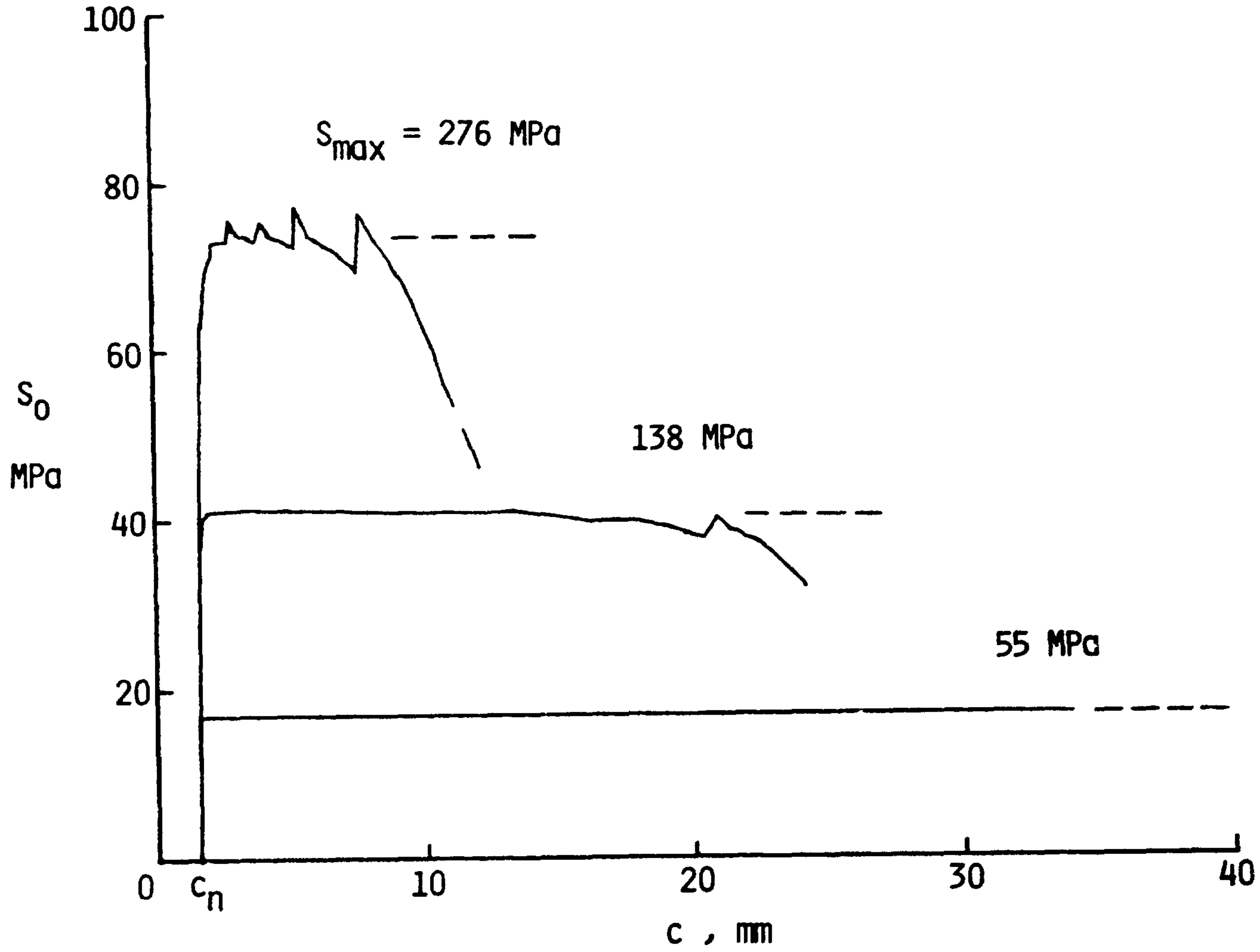

FIG. 7 - Calculated crack-opening stresses as a function of crack length under constant-amplitude loading (R = 0).

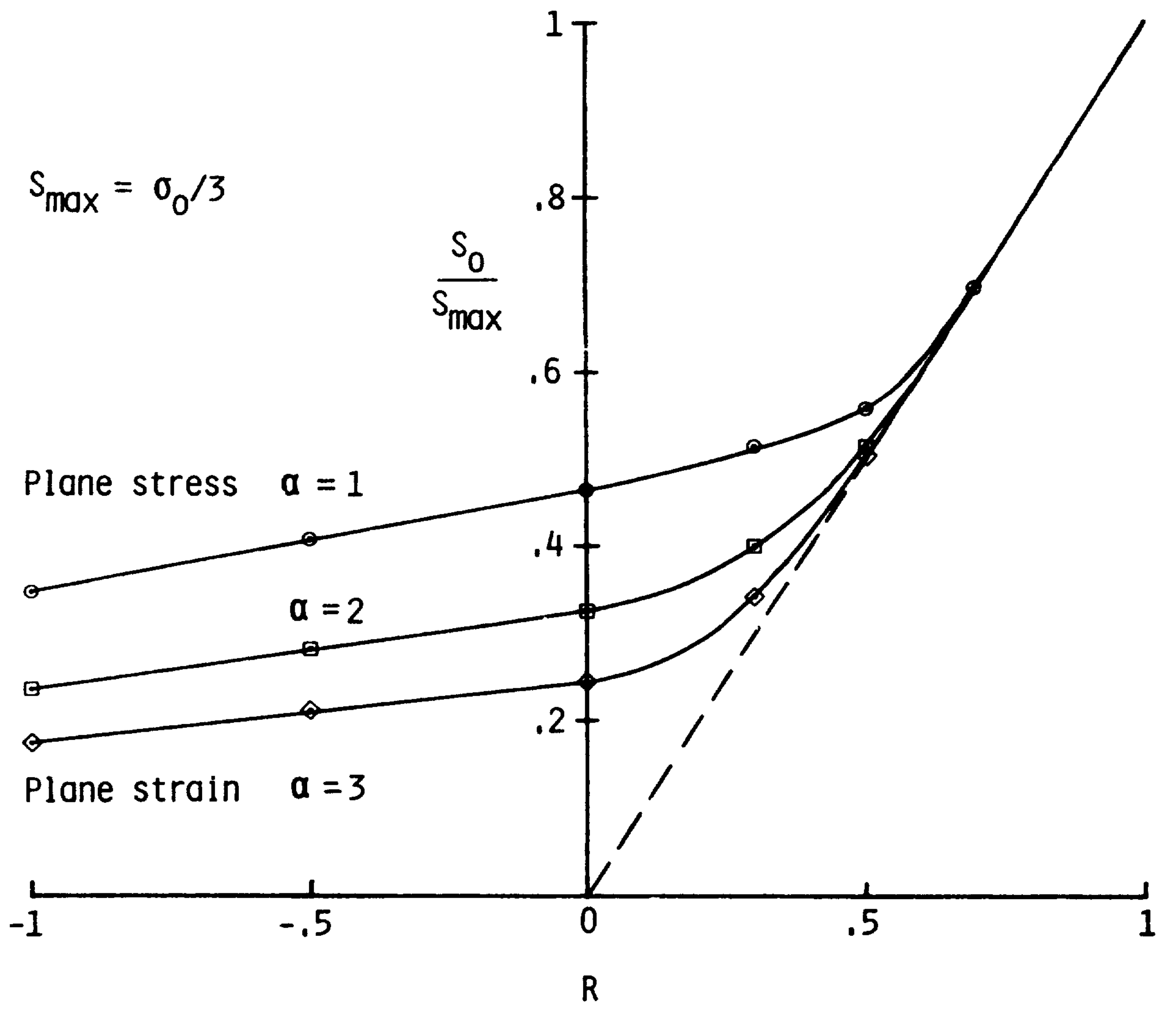

FIG. 8 - Normalized crack-opening stresses as a function of R ratio under constant-amplitude loading for simulated plane-stress and plane-strain conditions.

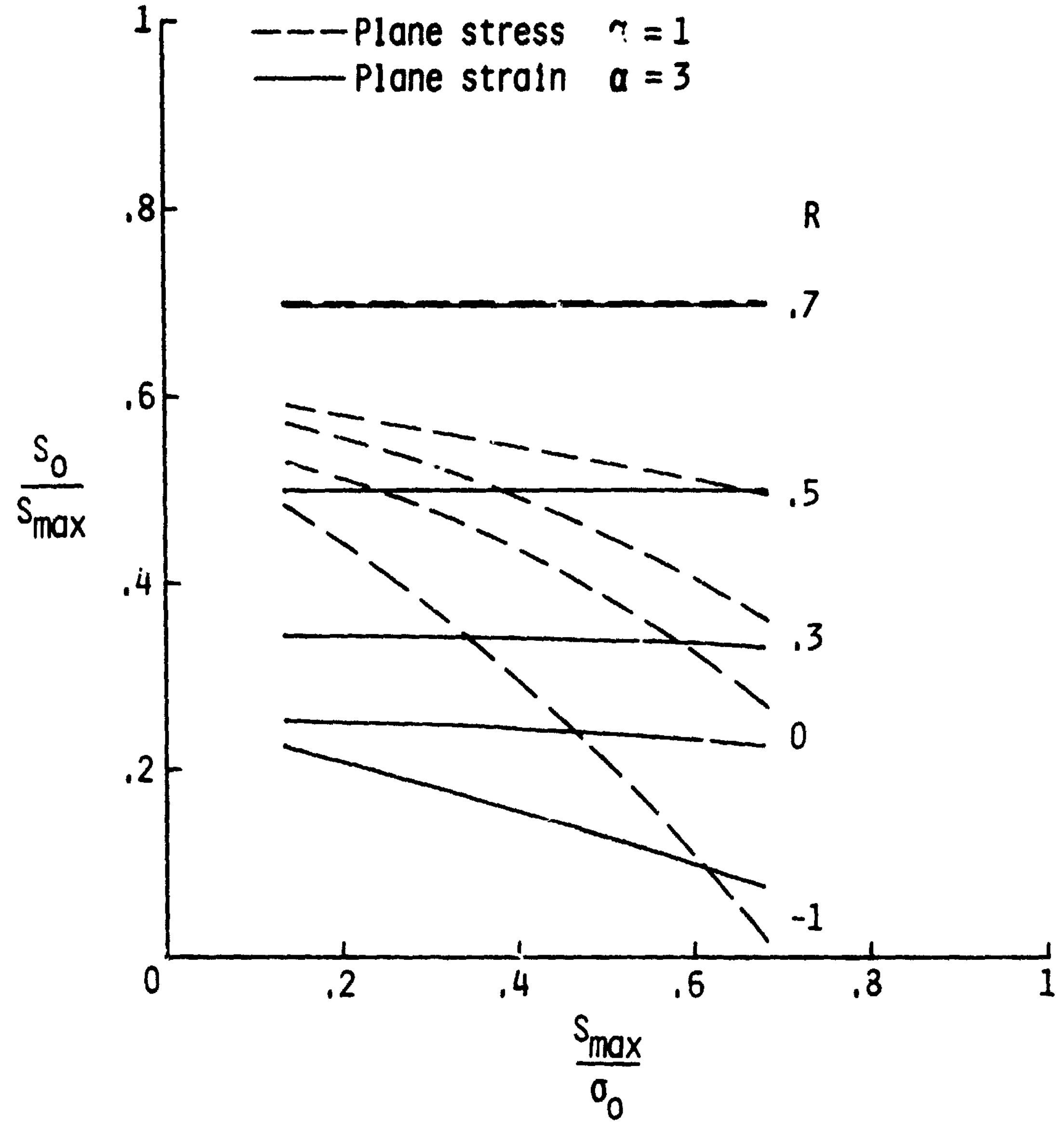

FIG. 9 - Normalized crack-opening stresses as a function of stress level for several R ratios.

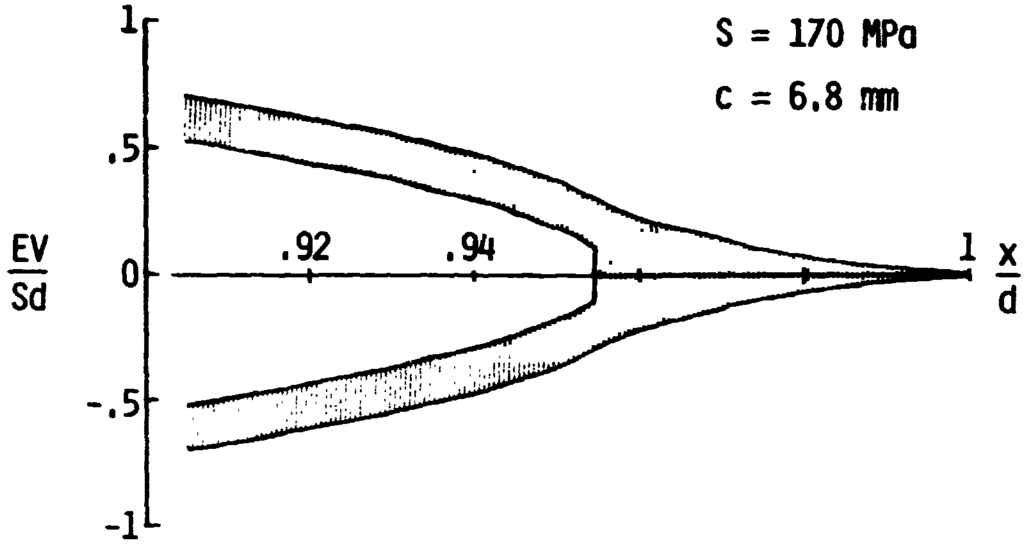

(a) Displacement profile at a high load

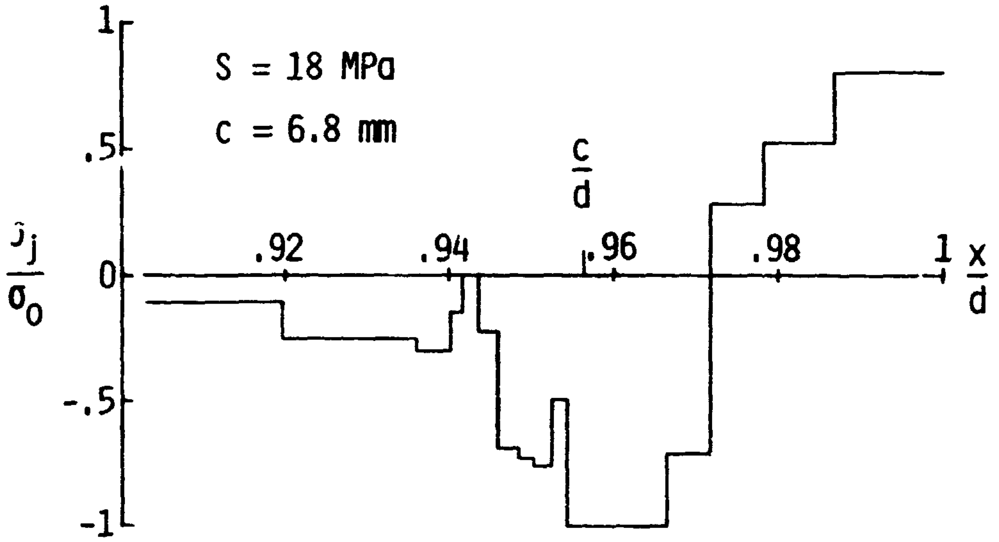

(b) Contact stresses at a low load

FIG. 10 - Crack-surface displacements and contact stresses under typical aircraft spectrum loading.

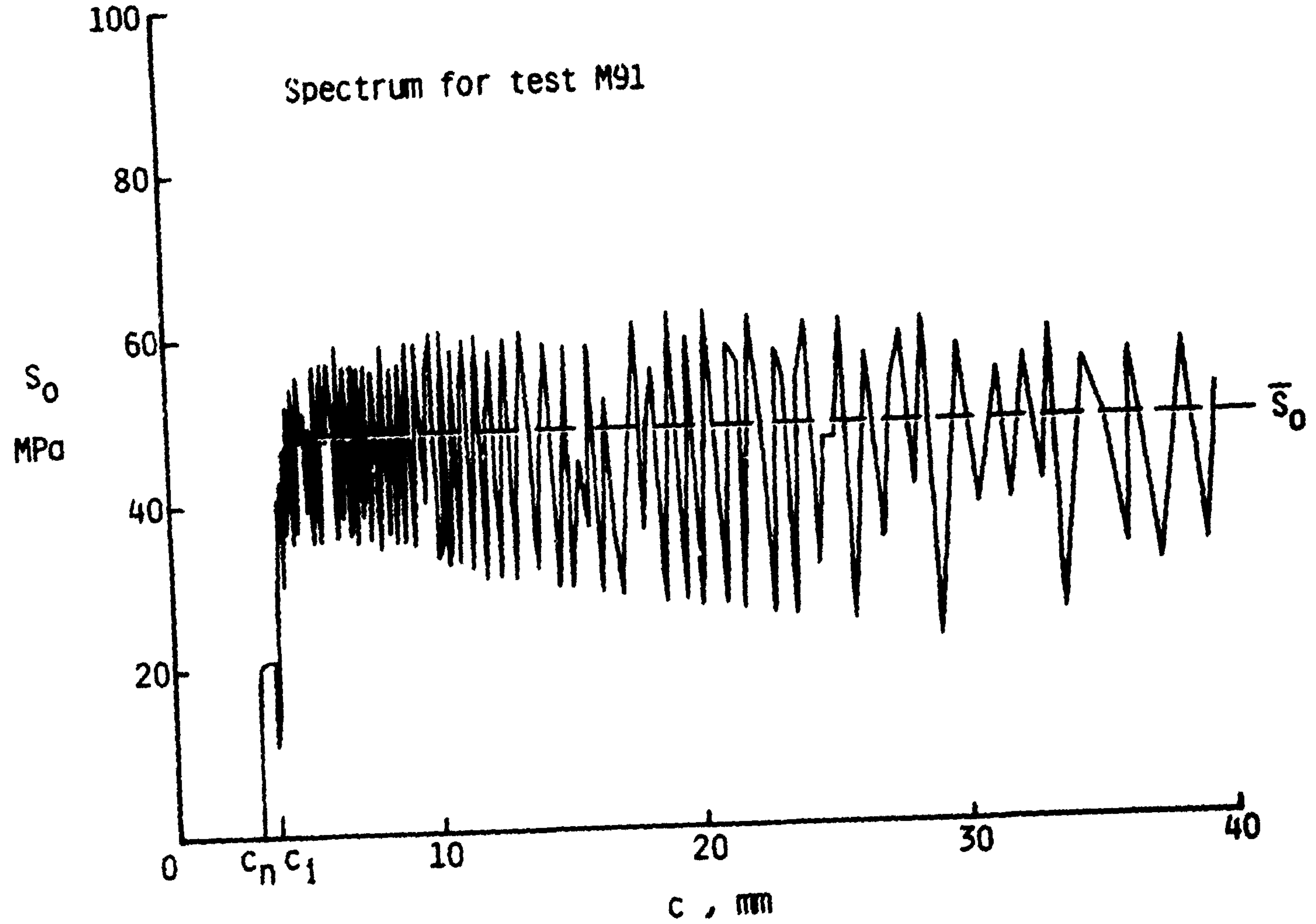

FIG. 11 - Calculated crack-opening stresses as a function of crack length under typical aircraft spectrum loading.

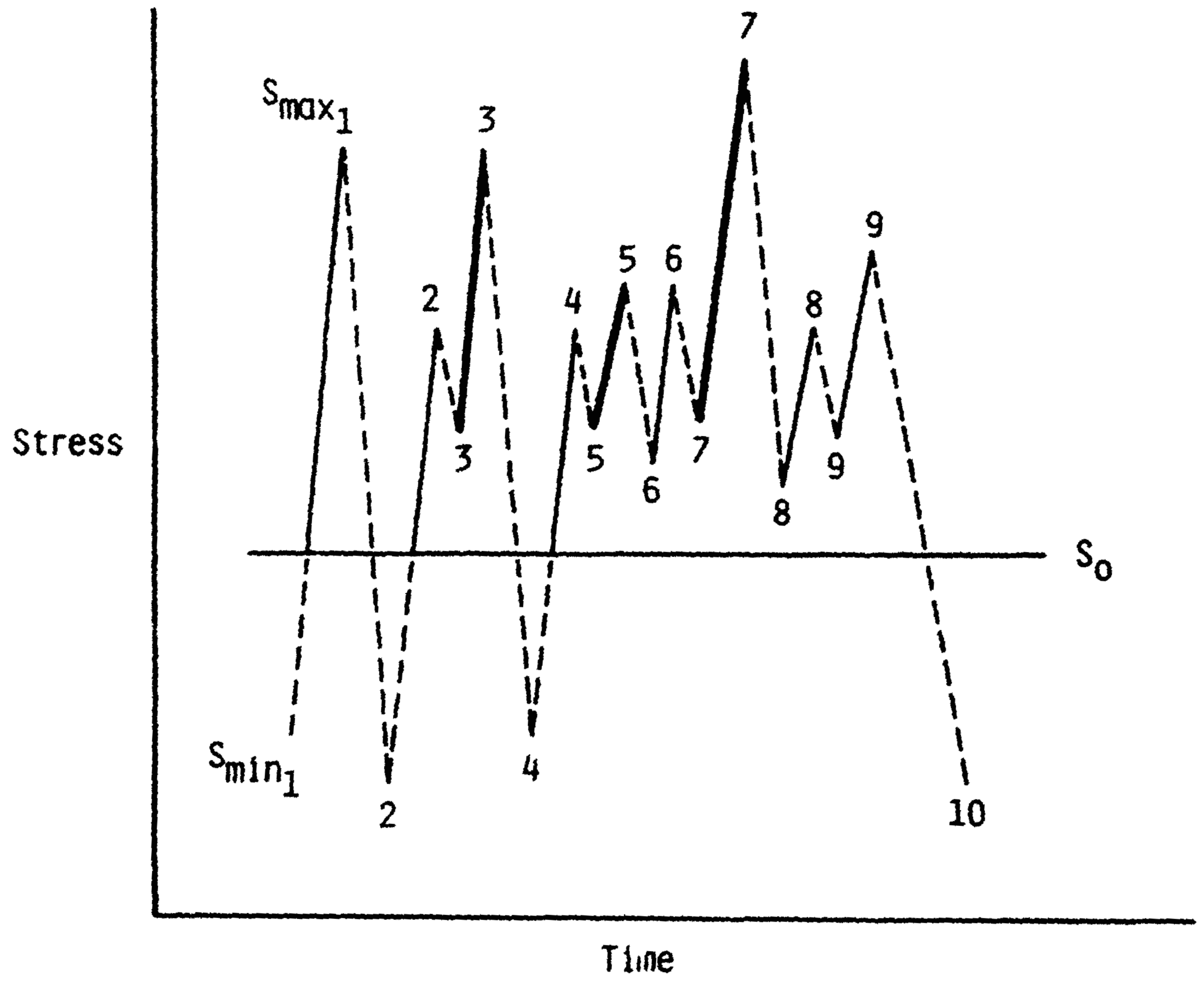

FIG. 12 - Variable-amplitude load history.

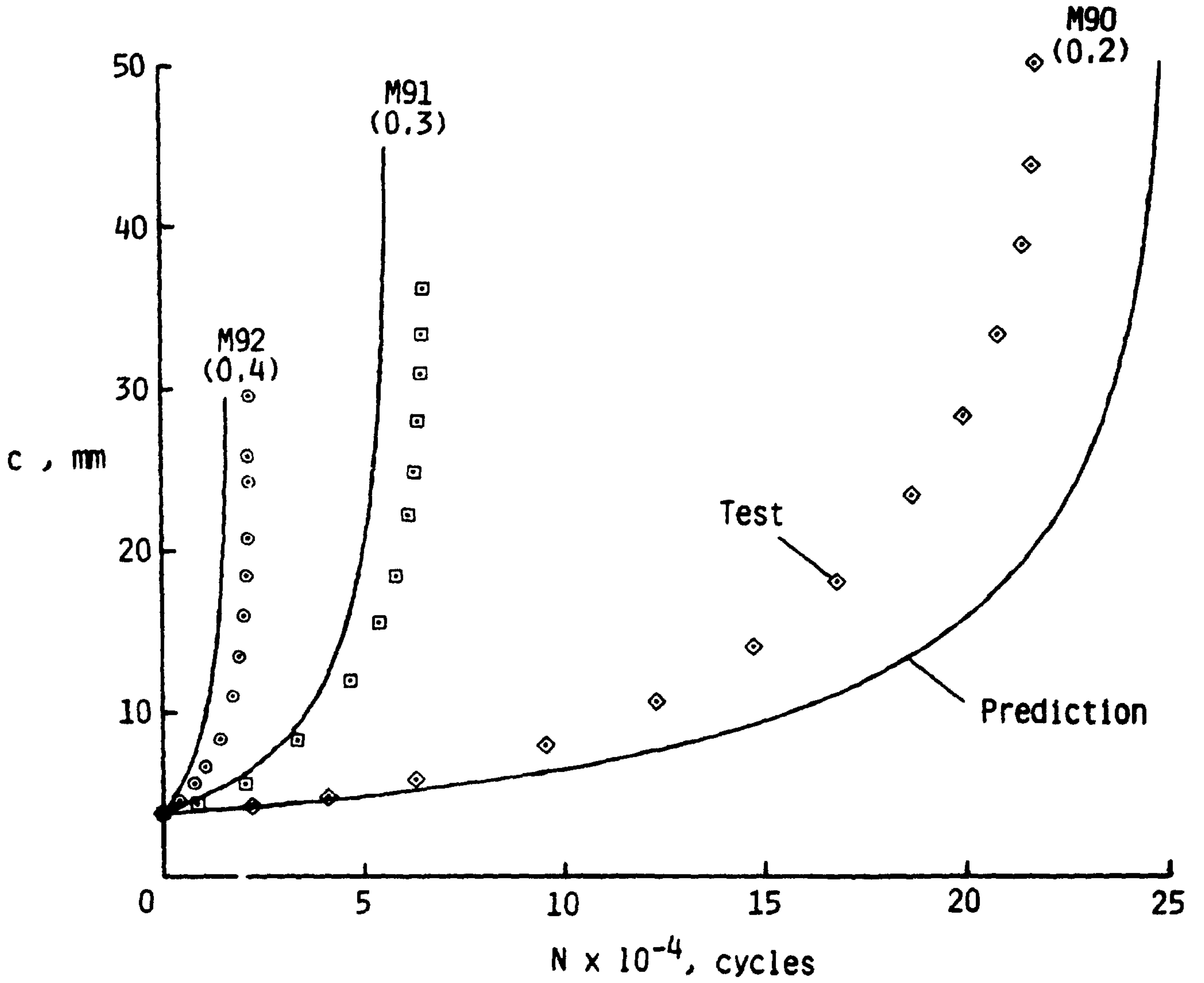

FIG. 13 - Comparison of experimental and predicted crack-length-against-cycles curves for spectrum loading.

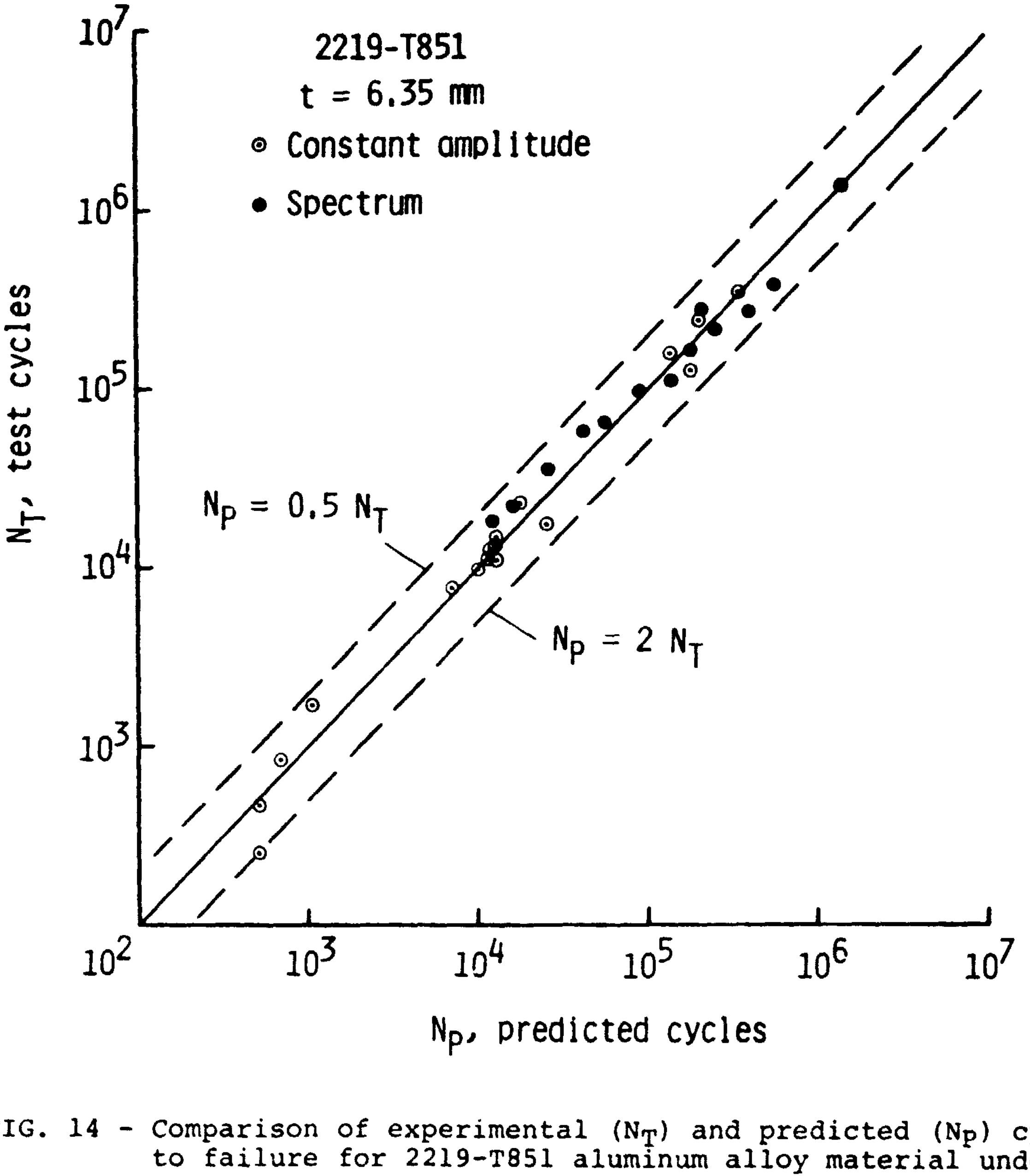

FIG. 14 - Comparison of experimental (N_T) and predicted (N_p) cycles to failure for 2219-T851 aluminum alloy material under constant-amplitude and spectrum loading.

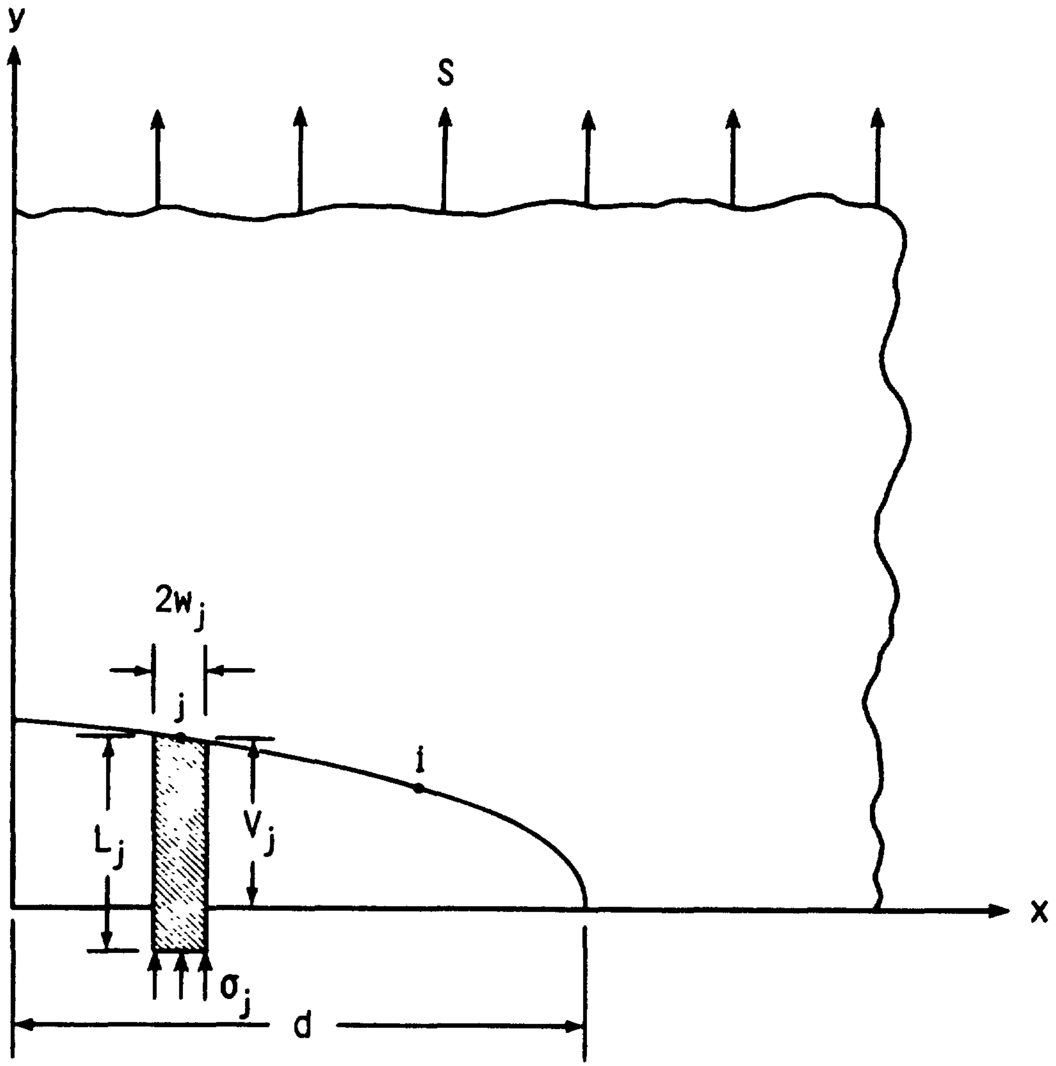

FIG. 15 - Schematic of loading and coordinate system used in the analytical closure model.

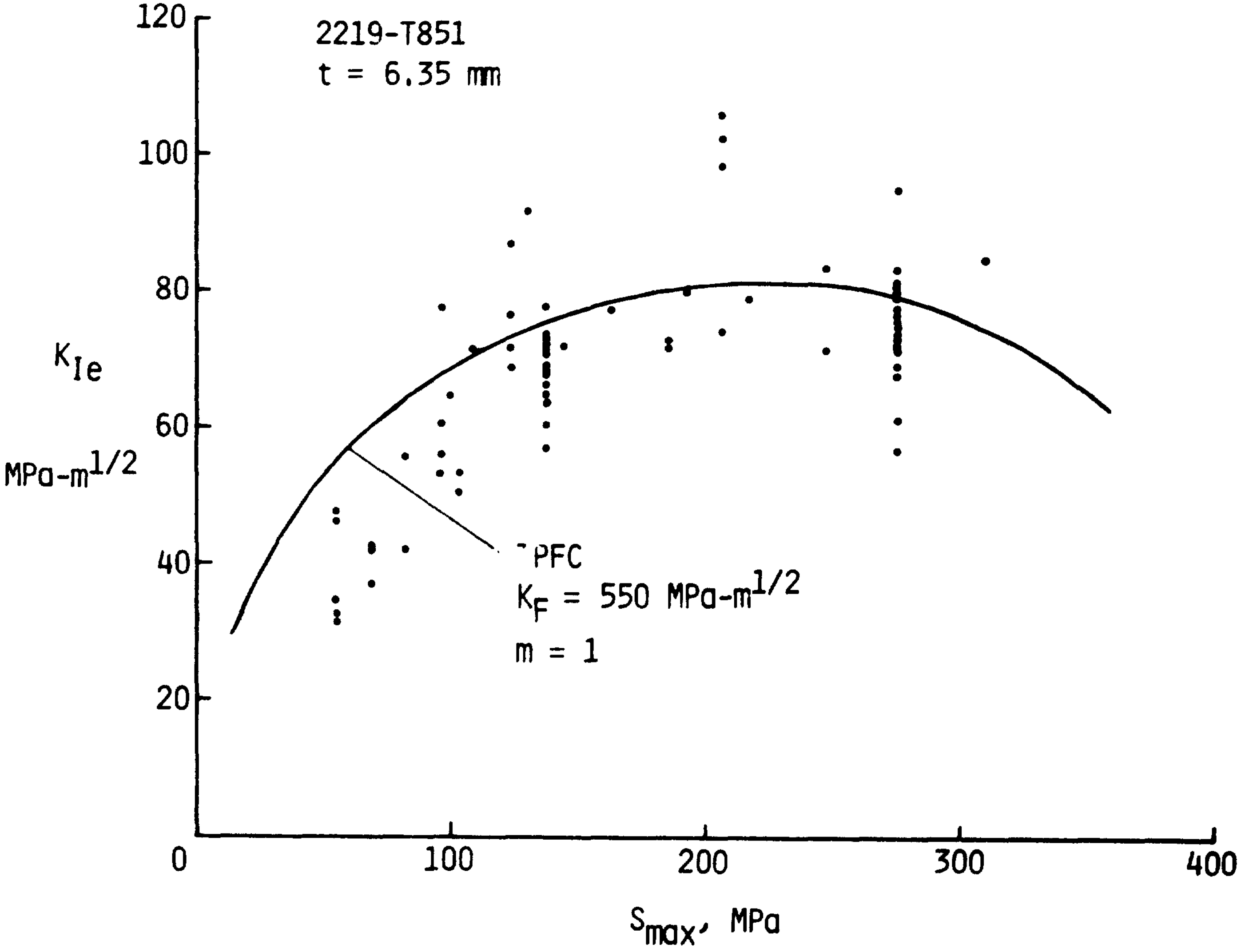

FIG. 16 - Comparison of experimental and calculated stress-intensity factors at failure under cyclic loading.